Analytical Investigation of the Dynamics of Tethered Constellations in Earth Orbit (Phase II)

Contract NAS8-36606

Quarterly Report #6

For the period 22 June 1986 through 21 September 1986

Principal Investigator

Dr. Enrico C. Lorenzini

October 1986

Prepared for
National Aeronautics and Space Administration
Marshall Space Flight Center, Alabama 35812

Smithsonian Institution
Astrophysical Observatory
Cambridge, Massachusetts 02138

The Smithsonian Astrophysical Observatory
is a member of the
Harvard-Smithsonian Center for Astrophysics

Analytical Investigation of the Dynamics of Tethered Constellations in Earth Orbit (Phase II)

Contract NAS8-36606

Quarterly Report #6

For the period 22 June 1986 through 21 September 1986

Principal Investigator
Dr. Enrico C. Lorenzini

Co-Investigators
Mr. David A. Arnold
Mr. Mario Cosmo
Dr. Mario D. Grossi

October 1986

Prepared for
National Aeronautics and Space Administration
Marshall Space Flight Center, Alabama 35812

Smithsonian Institution
Astrophysical Observatory
Cambridge, Massachusetts 02138

CONTENTS

Summary

This Quarterly Report addresses the following topics related to the dynamics of the 4-mass tethered system:

The development of damping algorithms for damping the out-of-plane libration of the system and the interaction of the out-of-plane control with the other degrees of freedom.

The development of environmental models to be added to the dynamics simulation computer code. The environmental models are specifically a new drag routine based on the Jacchia's 1977 model, a J_2 model and an accurate thermal model of the wire.

Figure Captions

Figure 1. In-plane and out-of-plane libration angles vs. time for a case in which the out-of-plane damping system is disactivated. The gains of the control laws are: $K_\theta=2$, $K_\varphi=0$.

Figure 2a-b. Dynamic response vs. time for a case in which a modified ($\bar{\varphi}$ = constant) yo-yo control law is adopted for out-of-plane libration control while the in-plane control system is disactivated. The gains of the control laws are: $K_\theta=0$, $K_\varphi=4$.

Figure 3a-b. The same as in Figure 2 except that this time the in-plane control system is activated. The gains of the control laws are: $K_\theta=1$, $K_\varphi=4$.

Figure 4a-i. The same as in Figure 2 (the in-plane control system is disactivated). The gains of the control laws are: $K_\theta=0$, $K_\varphi=10$.

Figure 5a-b. The same as in Figure 3. The gains of the control laws are: $K_\theta=0.1$, $K_\varphi=10$.

Figure 6a-r. Dynamic response vs. time for a case in which the standard yo-yo control law (variable $\bar{\varphi}$) is adopted for out-of-plane libration control. The in-plane control system is also activated. The gains of the control laws are: $K_\theta=0.2$, $K_\varphi=10$.

Figure 7a-b. Front-view and side-view respectively of the system under the conditions of Figure 6. The snapshots are every 100 sec for 36,000 sec. The x-axis scale is largely expanded.

Figure 8. Atmospheric density vs. altitude for different exospheric temperatures. The curves are obtained by means of an analytical fit of the Jacchia's 1977 model.

Figure 9a-d. Atmospheric density vs. time and exospheric temperature vs. time over one orbit at 450 km altitude and 28°.5 inclination. Figure 9a-b show the results for the sun at the Spring Equinox and Figure c-d for the sun at the Summer Solstice.

Figure 10. Acceleration components in the inertial reference frame due to the J_2 gravity term vs. time over one orbit at 450 km altitude and 28°.5 inclination.

Figure 11. Acceleration components in the orbiting reference frame due to the J_2 gravity term vs. time for the same conditions of Figure 10.

Figure 12. Schematic of the geometry of solar illumination for a tethered system.

Figure 13. Temperature vs. time over one equatorial orbit at 450 km altitude with illumination angle β=0 for a stainless steel tether of 2 mm diameter.

Figure 14. Same as in Figure 13 for a kevlar tether of 2 mm diameter.

1.0 INTRODUCTION

This is the sixth Quarterly Report submitted by SAO under contract NAS8-36606, "Analytical Investigation of the Dynamics of Tethered Constellations in Earth Orbit (Phase II)," Dr. Enrico C. Lorenzini, PI. This report covers the period from 22 June 1986 through 21 September 1986.

2.0 TECHNICAL ACTIVITY DURING REPORTING PERIOD AND PROGRAM STATUS

2.1 Algorithms For Damping Out-Of-Plane Librations

Damping of out-of-plane librations is achieved by controlling the lengths of the three tether segments connecting the four platforms. The out-of-plane librational dynamics of a multi-mass system can be modeled, with good approximation, by reducing the system to a two-mass system if the bowing of the former is small. The simplified equation of motion that describes the unperturbed, small out-of-plane librations of a two-mass tethered system is as follows:

$$\ell^2\ddot{\varphi} + 2\ell\dot{\ell}\dot{\varphi} + 4\ell^2\Omega^2\varphi = 0 \qquad (2.1.1)$$

For a two-mass tethered system the energy dissipated per cycle per unit mass is therefore given by ($\ell \simeq \ell_o$ for $\delta\ell \ll \ell_o$):

$$E_{D,\varphi} = -2\int_o^{\tau_\varphi} \ell\dot{\ell}\dot{\varphi}^2\, dt \simeq -2\ell_o\int_o^{\tau_\varphi} \dot{\ell}\dot{\varphi}^2 dt \qquad (2.1.1')$$

where τ_φ is the period of the out-of-plane libration equal to π/Ω. From simple physical considerations and also from equation (2.1.1′) it is immediately evi-

dent that the energy dissipated during an out-of-plane damping cycle does not depend upon the orbital rate Ω. The out-of-plane libration is in fact very weakly coupled with the longitudinal degrees of freedom, consequently tension control laws, which rely on such coupling, are poorly effective in damping out-of-plane librations. A simple mechanical equivalent of the out-of-plane dynamics of a tethered system is a pendulum of variable length on the ground (the pendulum has negligible Coriolis forces due to the Earth rotational rate and the librational frequency is approximately constant if the length variations are small). The yo-yo technique developed in reference [1] and [2] are perfectly suitable for damping the out-of-plane librations of a tethered orbital system. The same technique is on the contrary surpassed by the S-type [3] control law for damping the in-plane libration because the latter control law exploits the Coriolis forces generated by the orbital rate Ω. In order to clarify this point we can use equation (2.1.1′) for computing the energy dissipated by substituting into that equation various control laws. In the case of small damping we can assume that the libration over one cycle is approximately sinusoidal. We have therefore

$$\varphi \simeq \bar{\varphi} \sin\ (2\Omega t) \tag{2.1.2}$$

$$\dot{\varphi} \simeq 2\Omega\bar{\varphi} \cos\ (2\Omega t) \tag{2.1.3}$$

An ideal yo-yo control law (bang-bang type) can be expressed in formulae as follows:

$$\begin{aligned} \ell/\ell_o &= (1+K_\varphi\bar{\varphi}) \qquad \text{if sign}(\varphi) = \text{sign}\ (\dot{\varphi}) \\ \ell/\ell_o &= (1-K_\varphi\bar{\varphi}) \qquad \text{if sign}(\varphi) \neq \text{sign}\ (\dot{\varphi}) \end{aligned} \tag{2.1.4}$$

where $\bar{\varphi}$ is the amplitude of the out-of-plane libration. We can rewrite equation (2.1.1′) as follows:

$$E_{D,\varphi} = -\int_{o}^{\tau_\varphi} M_\varphi \, d\varphi = -\int_{o}^{\tau_\varphi} \dot{L}_\varphi \, d\varphi \qquad (2.1.5)$$

where M_φ is the out-of-plane component of the damping torque per unit mass and L_φ is the out-of-plane component of the angular momentum. By making use of equation (2.1.4) we finally have:

$$E_{D,\varphi} \simeq -2(\ell_{max}^2 - \ell_{min}^2)\dot{\varphi}_{max}^2 = -32\Omega^2\bar{\varphi}^3 K_\varphi \ell_o^2 \qquad (2.1.6)$$

The fractional damping of the φ degree of freedom can be obtained by equating the kinetic energy variation for that degree of freedom to the energy dissipated per cycle (per unit mass) given by equation (2.1.6). We have:

$$\Delta T_\varphi = E_{D,\varphi} \qquad (2.1.7)$$

or

$$2\ell_o^2\Omega^2 \, [(\bar{\varphi} - \Delta\bar{\varphi})^2 - \bar{\varphi}^2] \simeq 32\Omega^2\bar{\varphi}^3 K_\varphi \ell_o^2 \qquad (2.1.8)$$

After defining:

$$\delta\ell \doteq \ell_{max} - \ell_{min} = 2K_\varphi\bar{\varphi}\ell_o \qquad (2.1.9)$$

we obtain:

$$\frac{\Delta\bar{\varphi}}{\bar{\varphi}} \simeq 4\,\frac{\delta\ell}{\ell_o} \qquad \text{(ideal yo-yo, out-of-plane)} \qquad (2.1.10)$$

An ideal yo-yo control law, as expressed by equation (2.1.4) is unfeasible because it requires an infinite tether velocity. In actuality the ideal yo-yo control law is approximated by a sinusoidal control law (we call it smooth yo-yo) that can be defined as:

$$\ell/\ell_o = [1 + K_\varphi \bar{\varphi} \sin(4\Omega t)] \qquad (2.1.11)$$

By substituting equation (2.1.11), its derivative and equation (2.1.3) into equation (2.1.1′) we obtain:

$$E_{D,\varphi} \simeq -8\pi\Omega^2\ell_o^2\bar{\varphi}^3 k_\varphi \qquad (2.1.12)$$

After making use of equation (2.1.7) and of equation (2.1.9) we finally obtain:

$$\frac{\Delta\bar{\varphi}}{\bar{\varphi}} \simeq \pi \frac{\delta\ell}{\ell_o} \qquad \text{(smooth yo-yo, out-of-plane)} \qquad (2.1.13)$$

By using the smooth yo-yo instead of the ideal yo-yo we have therefore a decrease in damping effectiveness of roughly 20%.

A modification of the smooth yo-yo control law can be obtained by assuming that $\bar{\varphi}$ in equation (2.1.11) is constant and equal to the amplitude of the first out-of-plane libration cycle $\bar{\varphi}_1$. Consequently equation (2.1.13) is modified to

$$\frac{\Delta\bar{\varphi}}{\bar{\varphi}} \simeq \pi \frac{\bar{\varphi}_1}{\bar{\varphi}} \frac{\delta\ell}{\ell_o} \qquad (2.1.13')$$

The fractional damping is therefore increasing with the decrease of $\bar{\varphi}$. This result seems theoretically remarkable. In practice, however, the control of out-of-plane librations excites in-plane librations because the latter are

strongly coupled with tether length variations. This spill-over effect pumps the in-plane libration amplitude. By adopting the modified smooth yo-yo control law the spill-over does not decrease with $\bar{\varphi}$; the in-plane libration builds up. The in-plane control consequently tries to damp out the in-plane libration and by doing so impairs the effectiveness of the out-of-plane libration damping. In actuality therefore the result shown by equation (2.1.13′) is not achievable.

We want now to compare the in-plane libration damping with the out-of-plane libration damping. The simplified equation of motion that describes the unperturbed, small in-plane librations of a two-mass tethered system is as follows:

$$\ell^2\ddot{\theta} + 2\ell\dot{\ell}(\dot{\theta}-\Omega) + 3\ell^2\Omega^2\theta = 0 \qquad (2.1.14)$$

The energy dissipated over a cycle per unit mass is therefore given by ($\ell \simeq \ell_o$ for $\delta\ell \ll \ell_o$):

$$E_{D,\theta} = -2\int_o^{\tau_\theta} \ell\dot{\ell}(\dot{\theta}-\Omega)\dot{\theta}\,dt \simeq -2\ell_o\int_o^{\tau_\theta} \dot{\ell}(\dot{\theta}-\Omega)\dot{\theta}\,dt \qquad (2.1.15)$$

where τ_θ is the in-plane libration period equal to $2\pi/(\sqrt{3}\,\Omega)$. The equation, similar to equation (2.1.7), applicable to in-plane librations can be obtained by multiplying equation (2.1.14) by $\dot{\theta}$ and intergrating from o to τ_θ. Since $d\dot{\theta}^2/dt = 2\dot{\theta}\ddot{\theta}$ and $\ell \simeq \ell_o$ we obtain:

$$\ell_o^2\int_o^{\tau_\theta} d\dot{\theta}^2 + 2\ell_o\int_o^{\tau_\theta} \dot{\ell}(\dot{\theta}-\Omega)\dot{\theta}\,dt + 3\Omega^2\ell_o^2\int_o^{\tau_\theta}\theta\,d\theta = 0 \qquad (2.1.16)$$

Equation (2.1.16) can therefore be written as follows:

$$\Delta T_\theta^{\,rel} = E_{D,\theta} \qquad (2.1.17)$$

where ΔT_θ^{rel} stands for the kinetic energy of the θ degree of freedom relative to the LH-LV reference frame.

The smooth yo-yo control law for damping the in-plane libration is expressed as follows:

$$\ell/\ell_o = \left[1+K_\theta\bar{\theta}\sin(2\sqrt{3}\,\Omega t)\right] \qquad (2.1.18)$$

By following the same procedure adopted for computing the out-of-plane fractional damping but using equation (2.1.17) instead of (2.1.7) we arrive at the following result:

$$\frac{\Delta\bar{\theta}}{\bar{\theta}} \simeq \pi\,\frac{\delta\ell}{\ell_o} \qquad \text{(smooth yo-yo, in-plane)} \qquad (2.1.19)$$

This result stems from the fact that by using a yo-yo type control law we do not exploit the Coriolis forces generated by the orbital rate Ω. The fractional damping turns therefore to be the same for in-plane librations and out-of-plane librations; it would be completely different had we used a tension control law. The conclusion just reached prompted us to design the S-type control law for damping the in-plane libration. The S-type control law is formulated as follows:

$$\ell/\ell_o = (1-K_\theta\theta) \qquad (2.1.20)$$

The associated fractional damping, in the case of light damping, is given by:

$$\frac{\Delta\bar{\theta}}{\bar{\theta}} \simeq \frac{\pi}{\sqrt{3}}\,\frac{\delta\ell}{\ell_o\bar{\theta}} \qquad \text{(S-type, in-plane)} \qquad (2.1.21)$$

The most important feature is that the S-type control law provides a fractional damping that is independent of the amplitude $\bar{\theta}$. Heavy damping can be easily achieved with this type of control law even at small amplitude $\bar{\theta}$. In the case of heavy damping, however, equation (2.1.21) provides only a first order approximation of the fractional damping because the in-plane libration is no longer a pure sinusoid over a cycle; equation (2.1.21) gives an overestimation of the fractional damping in that case.

We have also computed the fractional damping for out-of-plane librations achieved by using other non linear control laws. Table 1 summarizes the fractional damping achievable vs. the various control laws shown in column one for the out-of-plane dynamics. Table 2 shows similar results for the in-plane dynamics.

Table 1

Out-of-Plane Libration Damping by Means of Tether-Length Control Law

Control Law	Mathematical Formulation	Fractional Damping
Ideal Yo-Yo	$\ell/\ell_o=(1+K_\varphi\bar{\varphi})$ if sign (φ) = $(\dot{\varphi})$ $\ell/\ell_o=(1-K_\varphi\bar{\varphi})$ if sign $(\varphi) \neq$ sign$(\dot{\varphi})$	$\frac{\Delta\bar{\varphi}}{\bar{\varphi}} \simeq 4\,\frac{\delta\ell}{\ell_o}$
Smooth Yo-Yo	$\ell/\ell_o = [1+K_\varphi\bar{\varphi}\sin(4\Omega t)]$	$\frac{\Delta\bar{\varphi}}{\bar{\varphi}} \simeq \pi\,\frac{\delta\ell}{\ell_o}$
Modified Smooth Yo-Yo	$\ell/\ell_o = [1+K_\varphi\bar{\varphi}_1\sin(4\Omega t)]$	$\frac{\Delta\bar{\varphi}}{\bar{\varphi}} \simeq \pi\,\frac{\bar{\varphi}_1}{\bar{\varphi}}\,\frac{\delta\ell}{\ell_o}$
$\varphi\dot{\varphi}$ Control Law	$\ell/\ell_o = [1+K_\varphi\varphi\dot{\varphi}]$	$\frac{\Delta\bar{\varphi}}{\bar{\varphi}} \simeq \pi\,\frac{\delta\ell}{\ell_o}$

Table 2

In-Plane Libration Damping by Means of Tether-Length Control Laws

Control Law	Mathematical Formulation	Fractional Damping
Ideal Yo-Yo	$\ell/\ell_o=(1+K_\theta\bar{\theta})$ if $\text{sign}(\theta)=(\dot{\theta})$ $\ell/\ell_o=(1-K_\theta\bar{\theta})$ if $\text{sign}(\theta)\neq(\dot{\theta})$	$\frac{\Delta\bar{\theta}}{\bar{\theta}} \simeq 4\,\frac{\delta\ell}{\ell_o}$
Smooth Yo-Yo	$\ell/\ell_o = [1+K_\theta\bar{\theta}\sin(2\sqrt{3}\,\Omega t)]$	$\frac{\Delta\bar{\theta}}{\bar{\theta}} \simeq \pi\,\frac{\delta\ell}{\ell_o}$
S-Type	$\ell/\ell_o = (1-K_\theta\theta)$	$\frac{\Delta\bar{\theta}}{\bar{\theta}} \simeq \frac{\pi}{\sqrt{3}}\,\frac{\delta\ell}{\ell_o\bar{\theta}}$

References to Section 2.1

1. Baker W.P. et al. "Tethered Subsatellite Study," NASA TM X-73314, March, 1976.

2. Spenser T.M. "Atmospheric Perturbation and Control of a Shuttle/Tethered Satellite," Proceedings of the 8th IFAC Symposium, Automatic Control in Space, 1980.

2.2 Simulation Runs With/Without Out-Of-Plane Libration Damping Algorithms

The previous section dealt with the yo-yo damping technique for a two-mass tethered system. In this section we generalize it to a four-mass tethered system. As already shown for the in-plane control system in Quarterly Report No. 5 Section 2.4 the generalization is readily implemented by controlling the three tether segments proportionally to their unstretched lengths. In formulae

$$\begin{aligned} \ell_{1c} &= \ell_{01}\ (1 - K_\theta\theta + K_{\epsilon I1}\epsilon_{I1}/\ell_{01} + \ell_{DLOL}) \\ \ell_{2c} &= \ell_{02}\ (1 - K_\theta\theta + K_{\epsilon I2}\epsilon_{I2}/\ell_{03} - K_{\epsilon I1}\epsilon_{I1}/\ell_{02} + \ell_{DLOL}) \\ \ell_{3c} &= \ell_{03}\ (1 - K_\theta\theta - K_{\epsilon I2}\epsilon_{I2}\ell_{02}/\ell_{03}^{\,2} + \ell_{DLOL}) \end{aligned} \qquad (2.1.22)$$

Equations (2.1.22) are similar to equations (2.4.3) of Quarterly Report No. 5 except for the term ℓ_{DLOL} that is the tether length variation per unit length for the out-of-plane libration control. The variable ℓ_{DLOL} depends on the particular control law adopted.

Several simulation runs have been done in order to derive a reasonable technique for damping the out-of-plane oscillations. The smooth yo-yo control law has been extensively tested either in the standard (variable $\bar{\varphi}$) or in the modified version (constant $\bar{\varphi}$). The in-plane libration angle θ and the out-of-plane libration angle φ are shown in Figure 1 for a case in which the in-plane libration control is activated (K_θ=2) while the out-of-plane libration control is off (K_φ=0). Notice that the in-plane libration is very well damped and that the in-plane control does not spill over the out-of-plane libration. The vice-versa is not true. The second simulation was run by adopting K_θ=0 (in-plane control off) and K_φ=4 in the modified smooth yo-yo control law. Figure 2a shows the out-of-plane angle vs. time. The fractional damping (for light damp-

ing: fractional damping $\simeq$ logarithmic decrement = Δ; damping ratio $\simeq \frac{\Delta}{2\pi}$) of the angle φ is approximately 11%. Figure 2b shows the in-plane angle and the out-of-plane angle vs. time for the same case. This figure clearly shows the spill of the out-of-plane control over the in-plane libration. The amplitude of the in-plane angle is building up. A third simulation was run in order to address the issue of the back action of the in-plane control over the out-of-plane damping. The control law adopted for the out-of-plane libration is the same of the previous run with the same gain $k_\varphi = 4$. The in-plane control is activated with a gain $k_\theta = 1$ in the S-type control law. Figure 3a shows the out-of-plane angle vs. time for a time duration of 5000 sec. Because of the activation of the in-plane control the out-of-plane damping is reduced from 11% to 6.5%. The in-plane amplitude growth due to the spill-over is, on the contrary, reduced from 2° to 1° as shown in Figure 3b. In the fourth simulation run K_θ=0 and K_φ=10. This simulation has been run for 10,000 sec to show better the build-up of in-plane librations. Figure 4a depicts the out-of-plane libration angle vs. time. A fractional damping $\simeq$ 26% has been achieved. The out-of-plane libration phase-plane, depicted in Figure 4b, stresses this result. Figure 4c shows the in-plane libration angle build-up (together with the out-of-plane angle vs. time) while Figure 4d depicts the phase-plane of the in-plane libration. The fractional tether length variation $\delta\ell/\ell_o$ for out-of-plane libration control is shown in Figure 4e (in the case of the modified smooth yo-yo, $\delta\ell/\ell_o$ has a constant amplitude). By substituting the values of $\delta\ell/\ell_o = 0.12$ (remember that $\delta\ell$ is a peak-to-peak variation) into equation (2.1.13′) for the first cycle (when $\varphi_1/\bar{\varphi} = 1$) we obtain a fractional damping $\Delta\bar{\theta}/\bar{\theta} = 38\%$ that is greater than the measured one (26%). The difference can be attributed to two different effects: 1) Equation (2.1.13′) and all the other similar equations are valid for light damping and they overestimate the damping if otherwise. 2) The tether elasticity deforms the eight-shaped damping cycle invoked by equation

(2.1.11). This latter effect is readily noticeable in Figure 4f that shows the trajectory of mass no. 1 with respect to the orbiting reference frame (located approximately at the system C.M.). For completeness Figure 4g and 4h show the in-plane and out-of-plane components respectively of the distances of the middle-masses from the straight line through the end-masses (lateral deflections). Figure 4i depicts the moduli of such distances. In the fifth simulation the same gain k_φ = 10 of the previous simulation was adopted for the out-of-plane libration control while K_θ was set equal to 0.1 in an attempt of limiting the in-plane oscillation growth without impairing the damping of out-of-plane librations. Figure 5a shows the out-of-plane libration angle vs. time. The fractional damping reduction is almost negligible: from 26% to 25%. Figure 5b shows the in-plane libration angle vs. time and the out-of-plane angle vs. time. The in-plane amplitude growth is reduced compared to the previous run. All the other features of this run are similar to the previous one. Because of the results obtained by adopting the modified yo-yo control law we decided to switch to the standard yo-yo (variable $\bar{\varphi}$) for the following simulations in order to reduce the spill-over due to the out-of-plane libration control.

The sixth simulation run adopts K_φ=10 in the standard yo-yo control law while K_θ is set equal to 0.2. This simulation has been run for 36,000 sec. Figure 6a shows the angle φ vs. time. The fractional damping is, at the beginning, around 17%. The fractional damping starts decreasing past 15000 sec. The variation is, however, non-monotonic: the fractional damping goes almost to zero around 30000 sec and goes up again to 6% at 32000 sec. Various sources can contribute to the deviation of the fractional damping behavior from equation (2.1.13): 1) the tether length variation for yo-yo control, as expressed in equation (2.1.11), has no frequency feedback; the controller goes slowly out of phase with the φ oscillation because of the frequency variation due to damping.

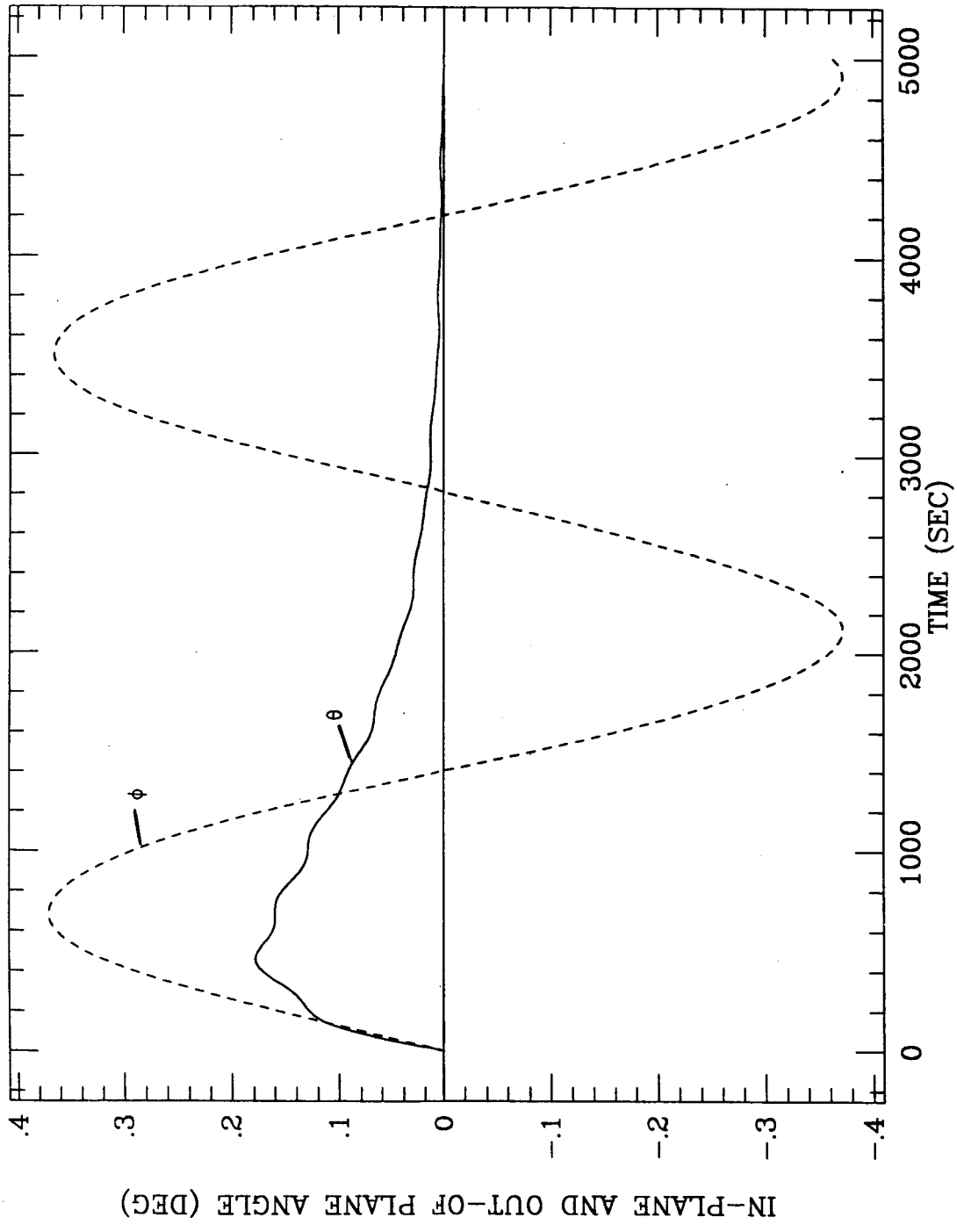
IN-PLANE AND OUT-OF PLANE ANGLE (DEG)
.4
.3
.2
.1
0
-.1
-.2
-.3
-.4
0
1000
2000
3000
4000
5000
TIME (SEC)
φ
θ

Figure 1.

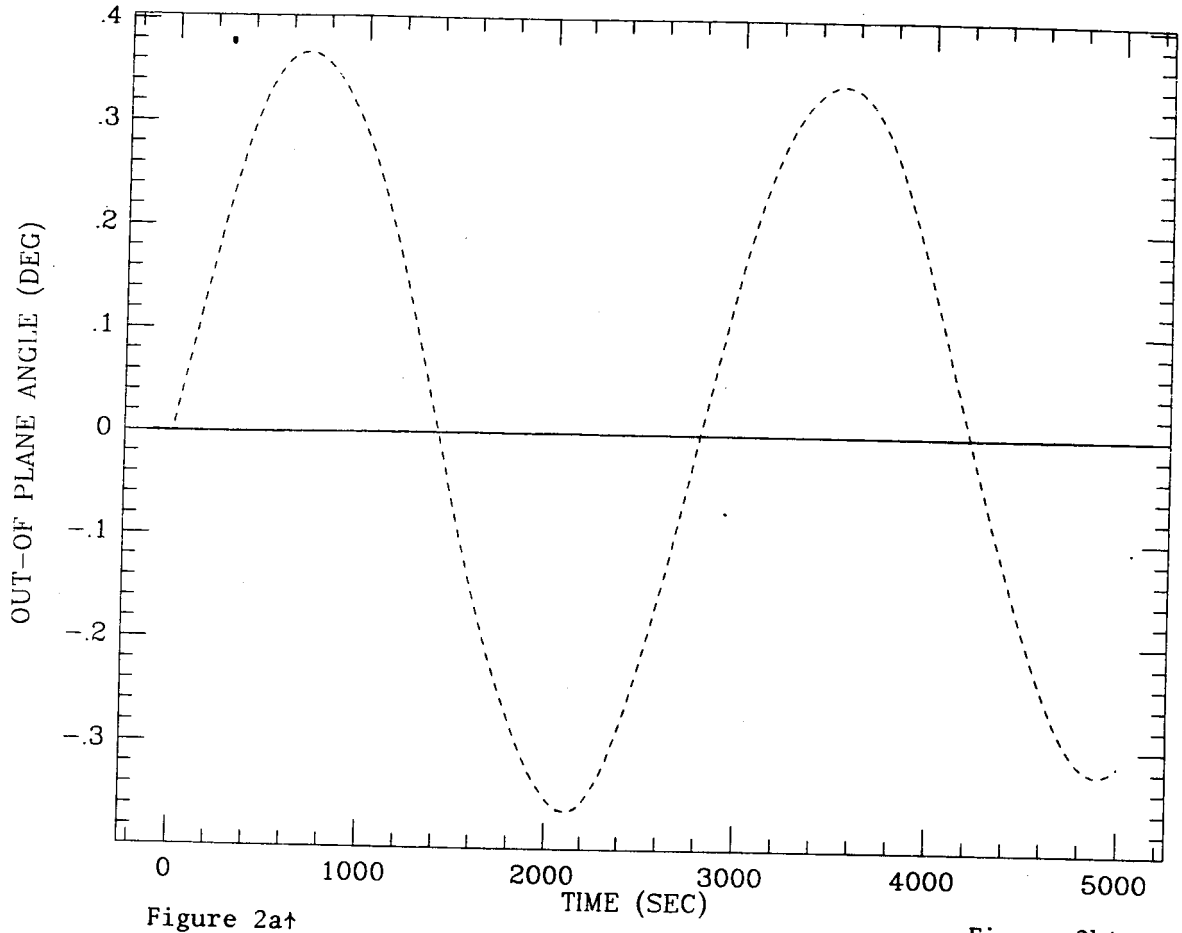

Figure 2a↑

Figure 2b↓

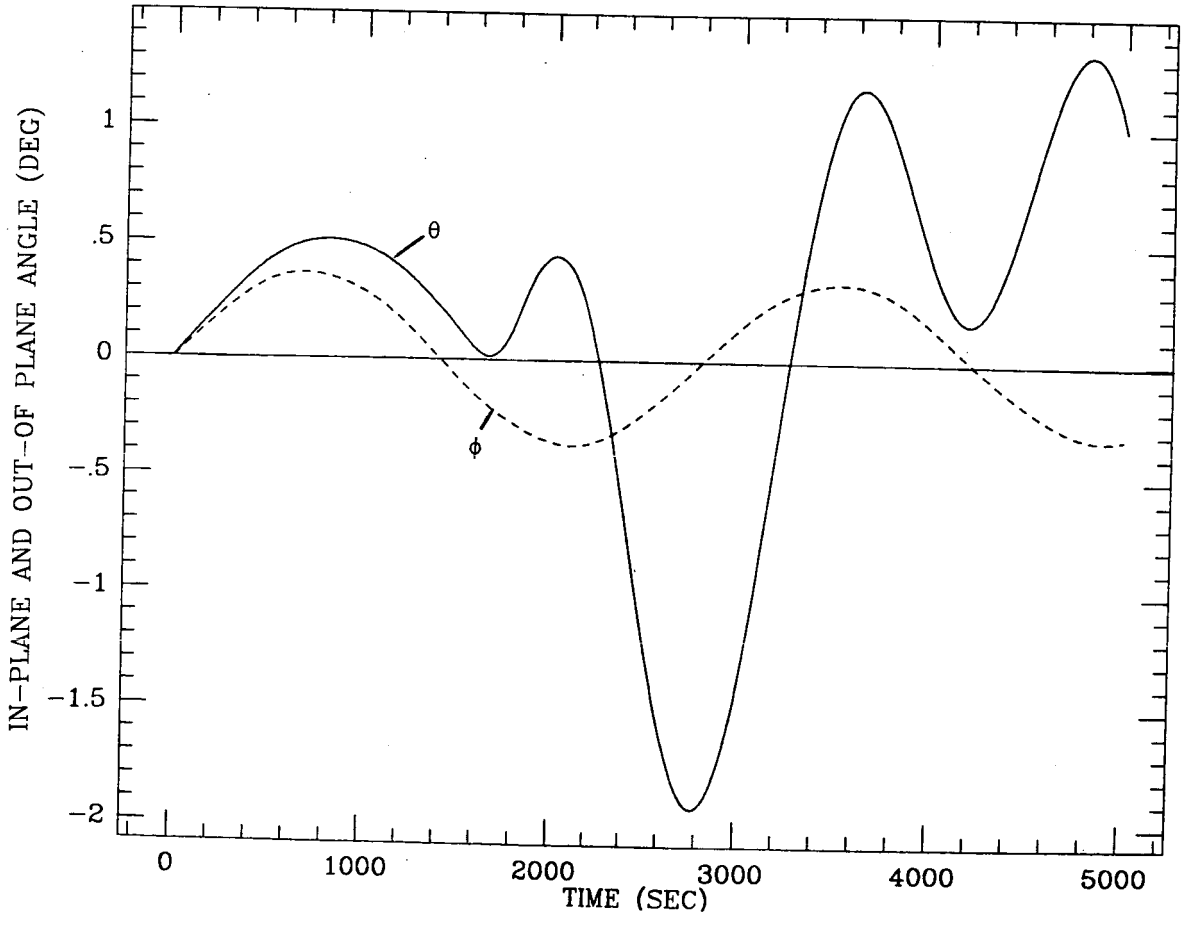

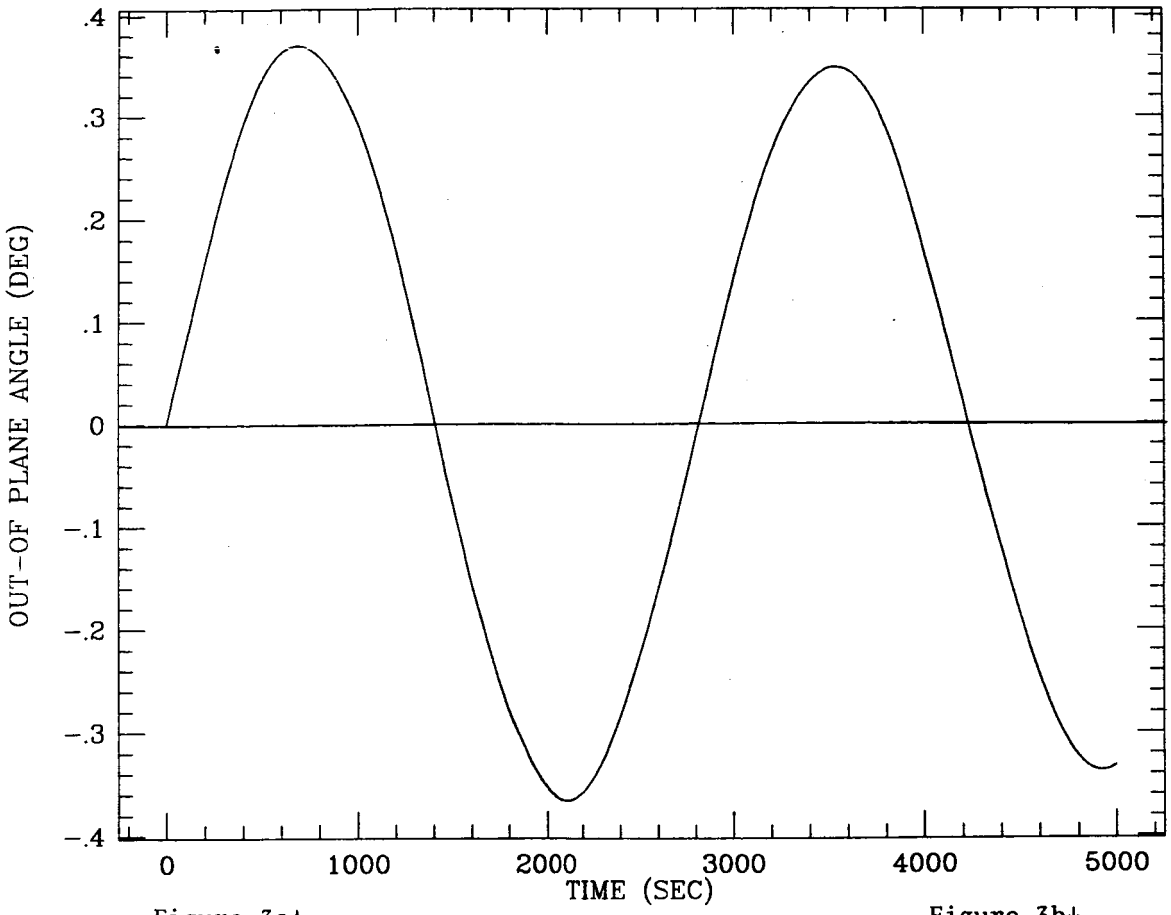

Figure 3a↑

Figure 3b↓

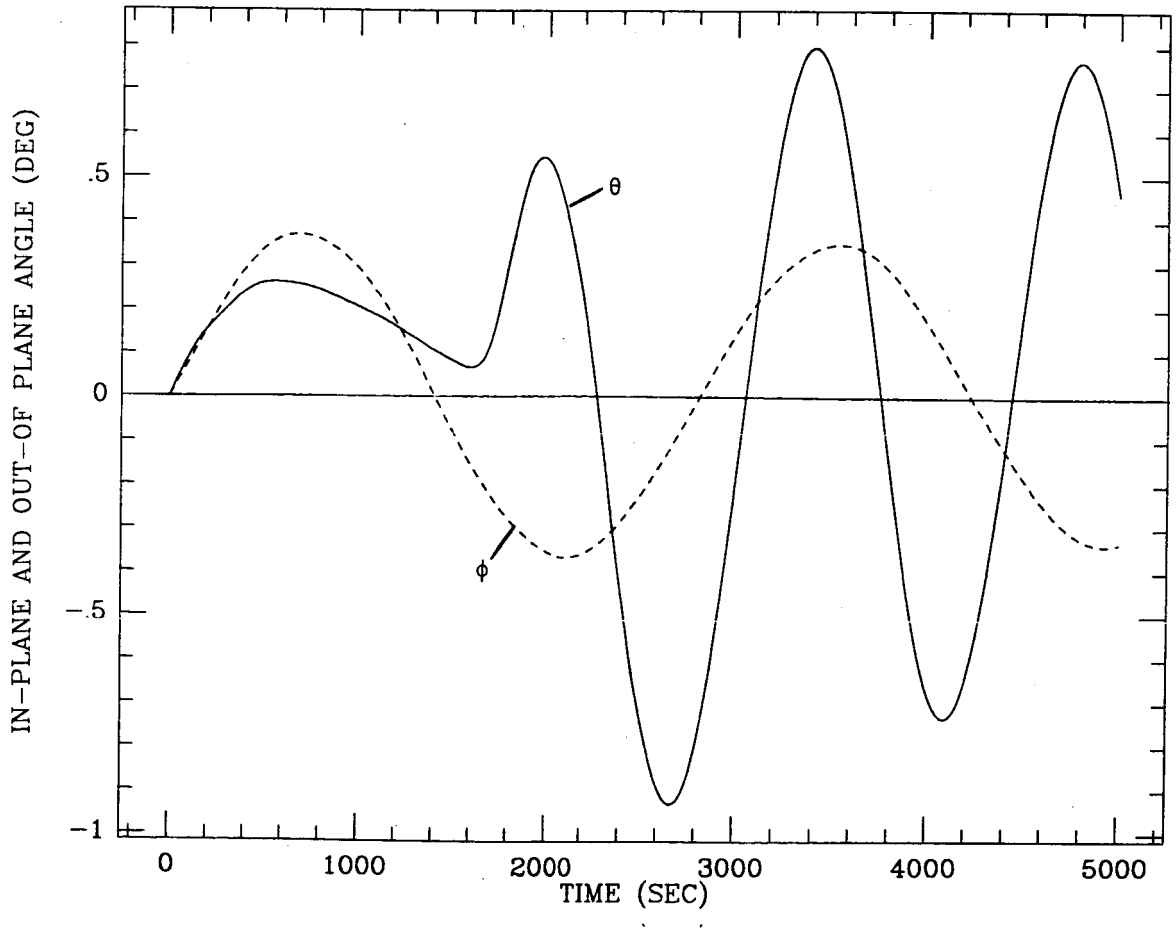

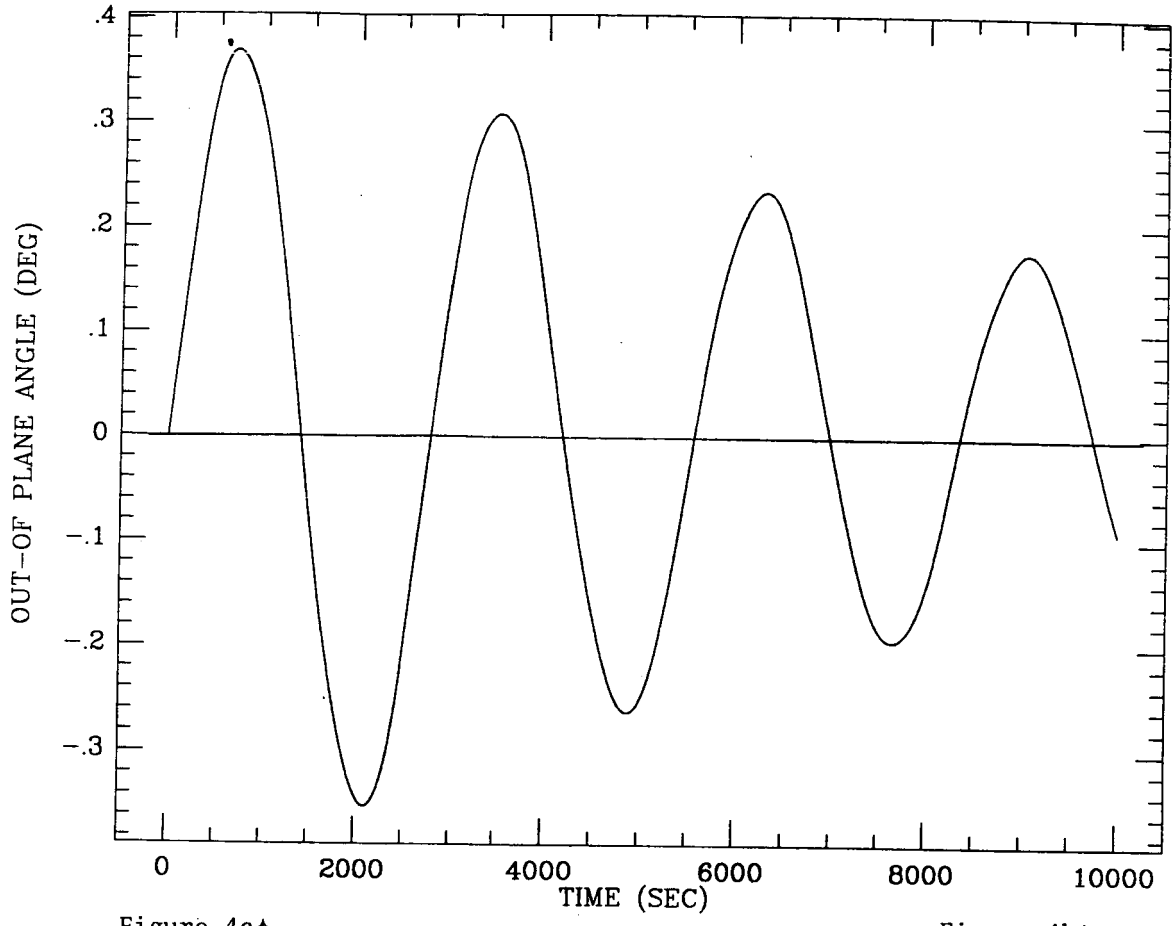

Figure 4a↑

Figure 4b↓

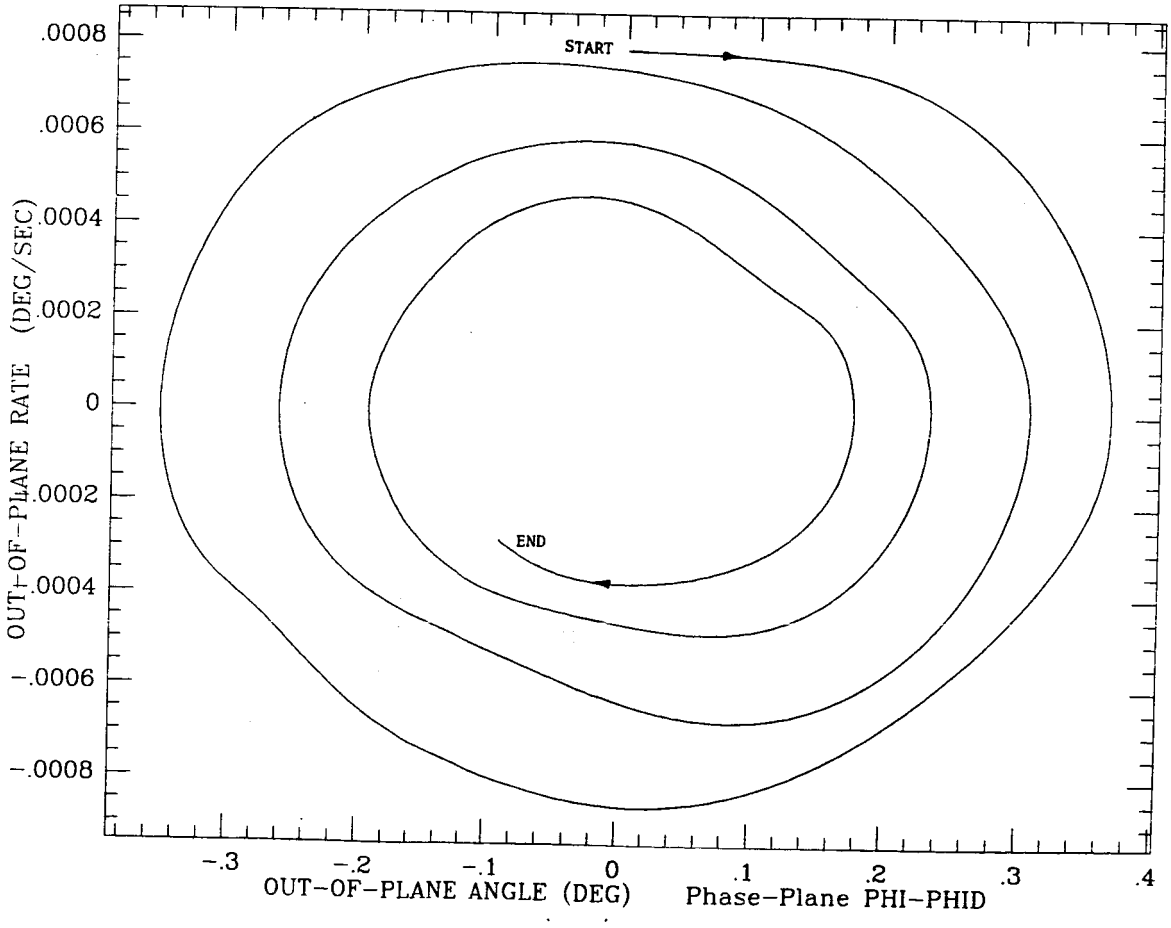

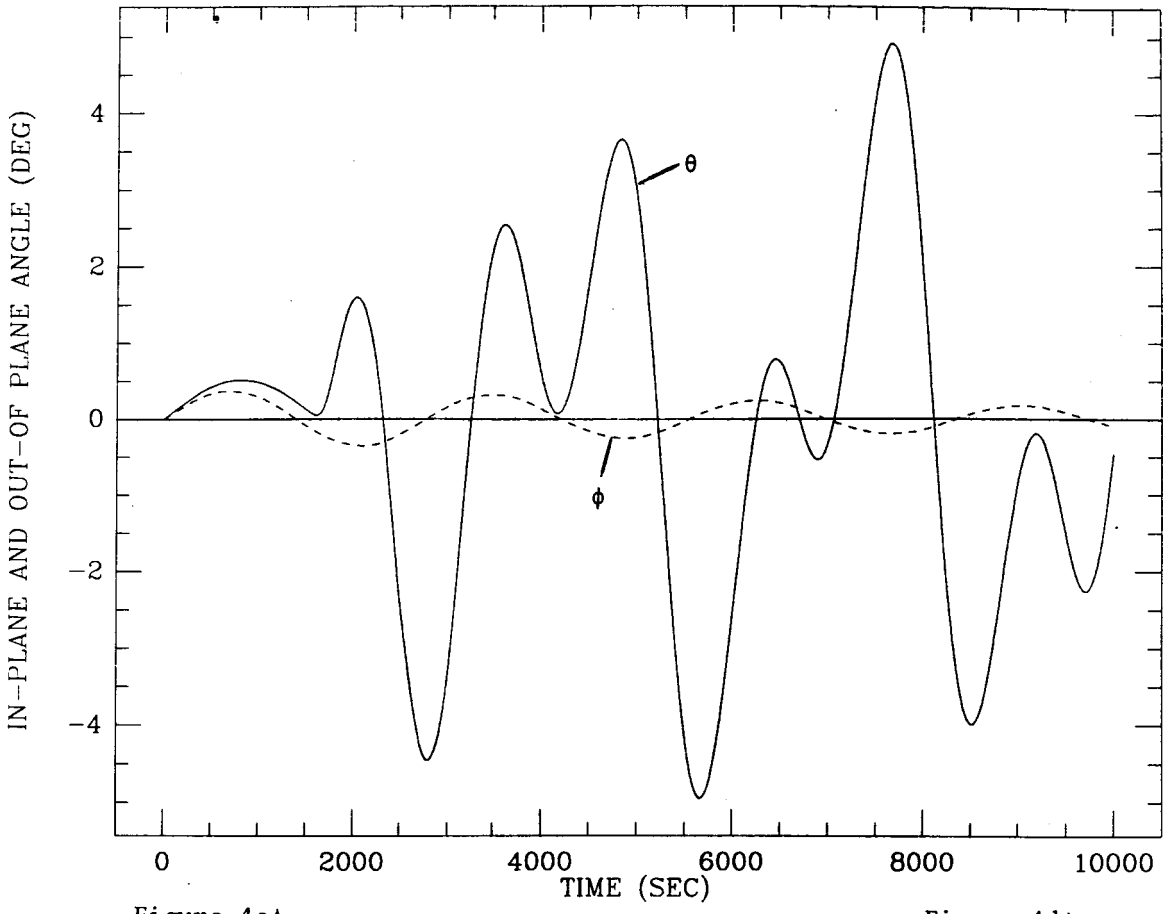

Figure 4c↑

Figure 4d↓

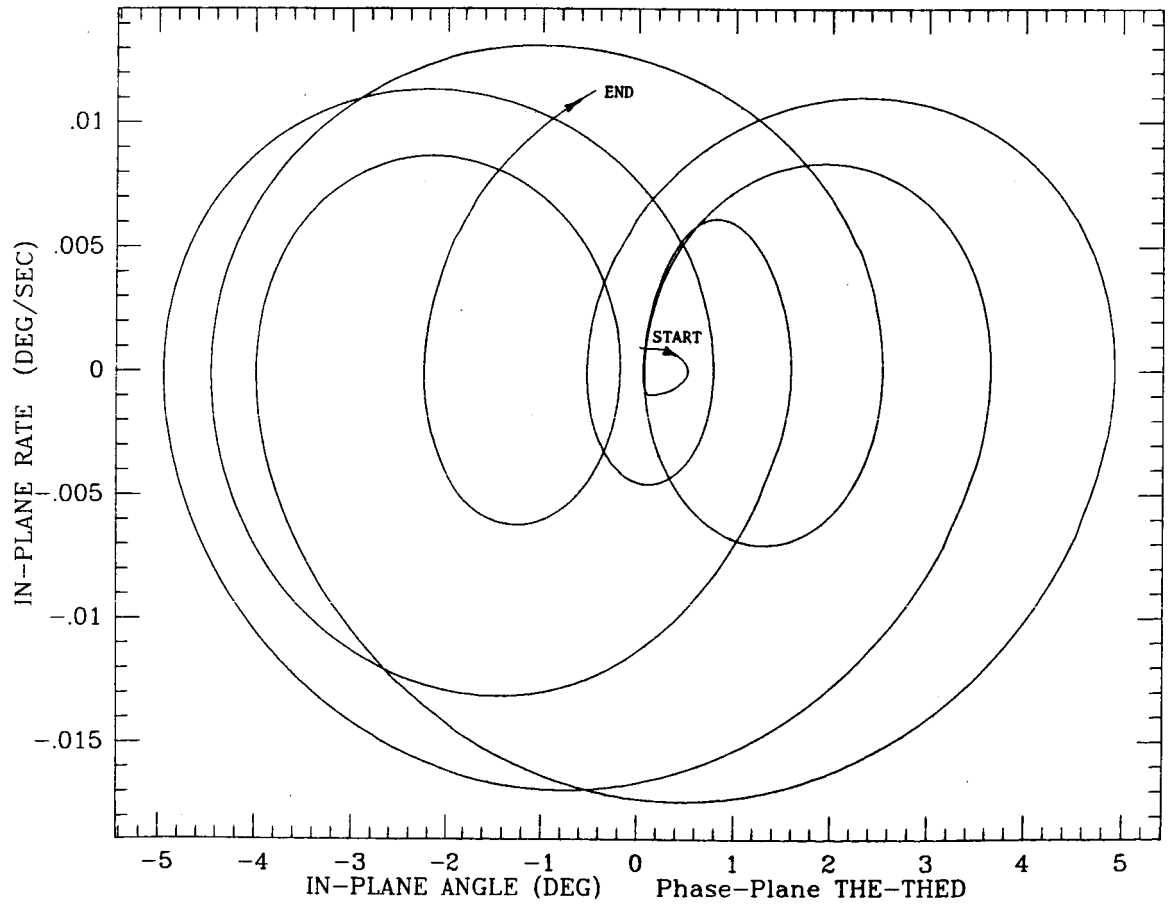

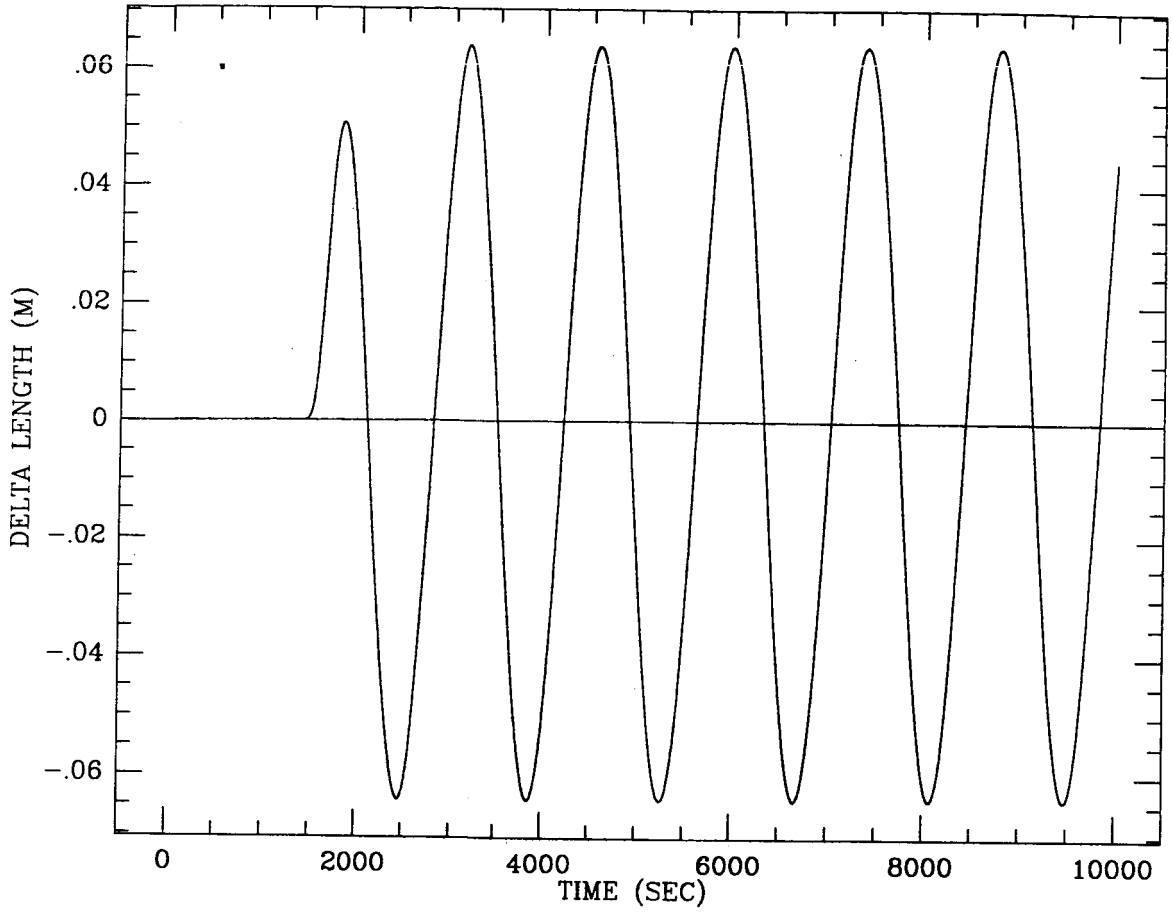

Figure 4e↑

Figure 4f↓

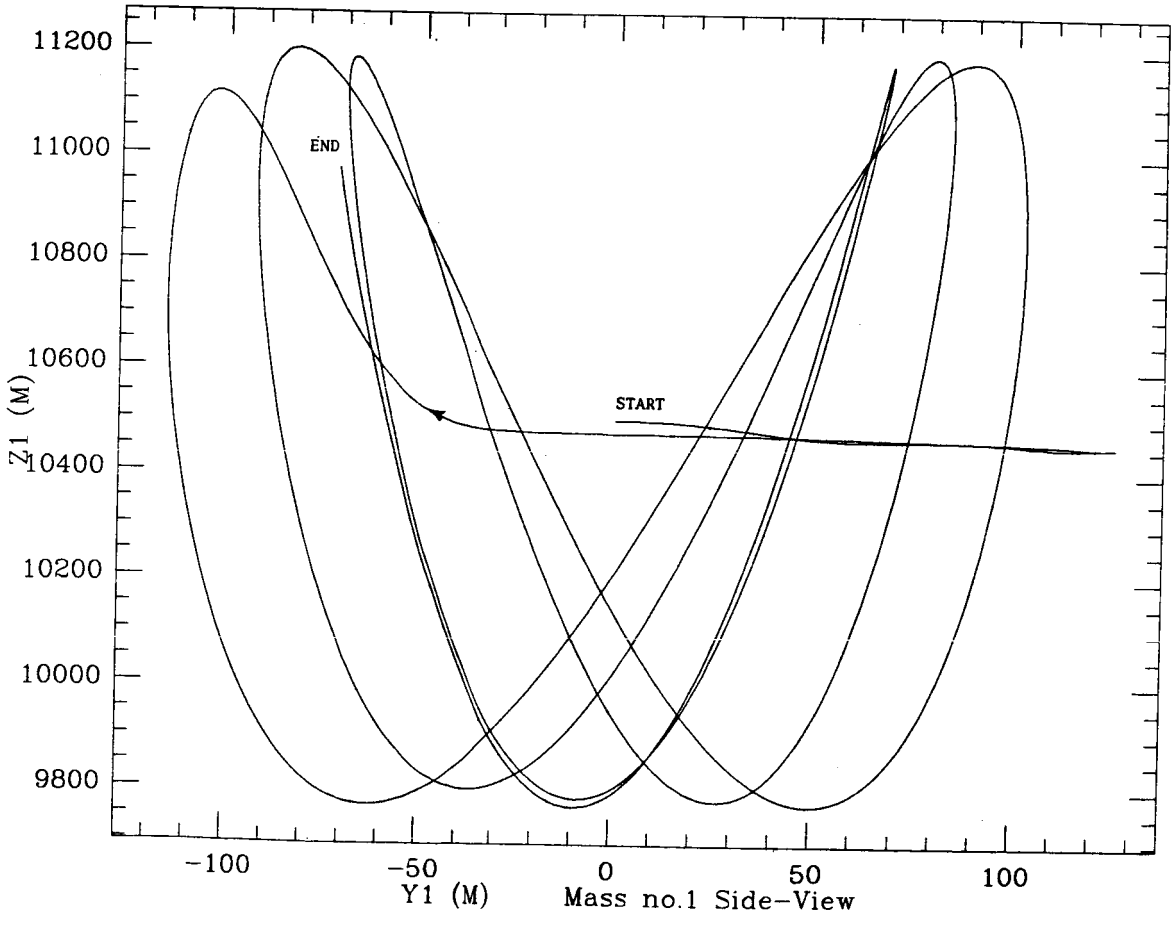

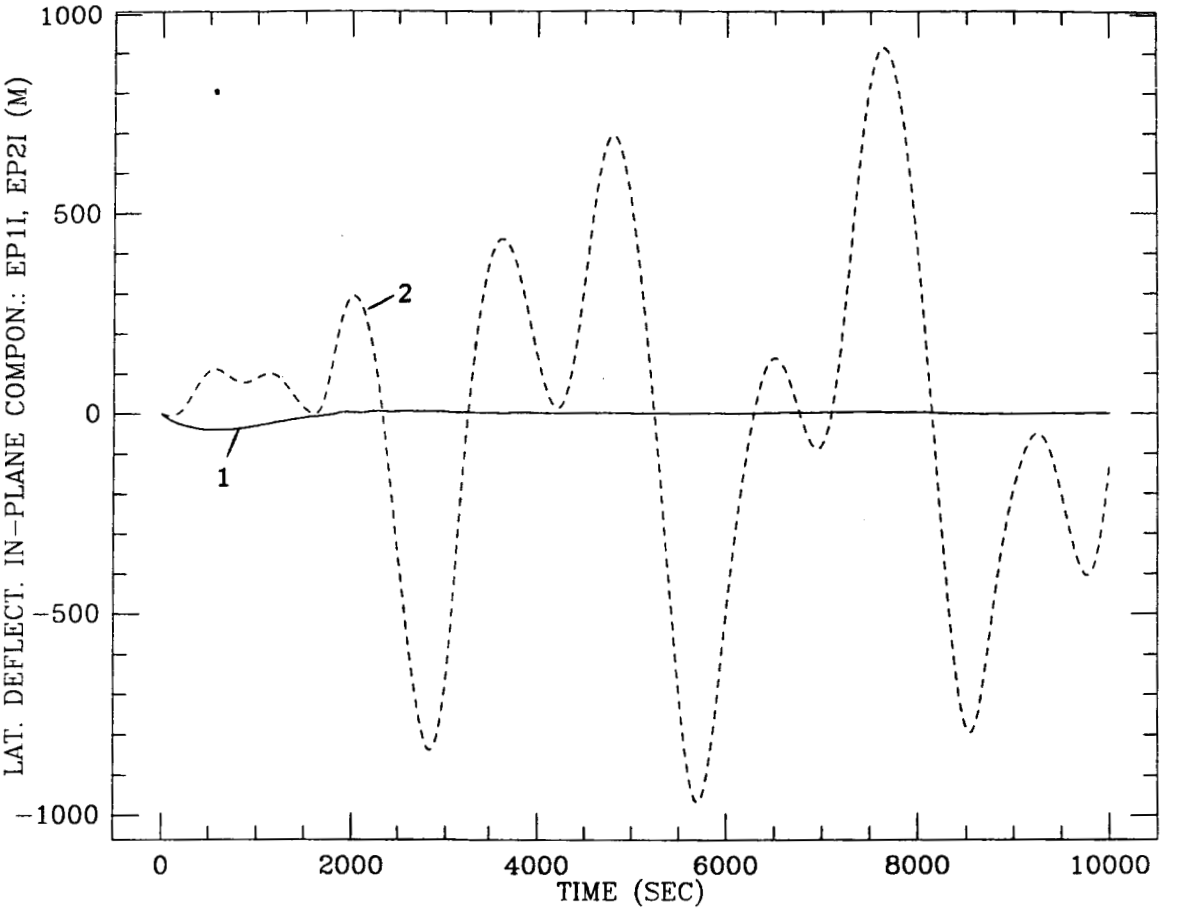

Figure 4g↑

Figure 4h↓

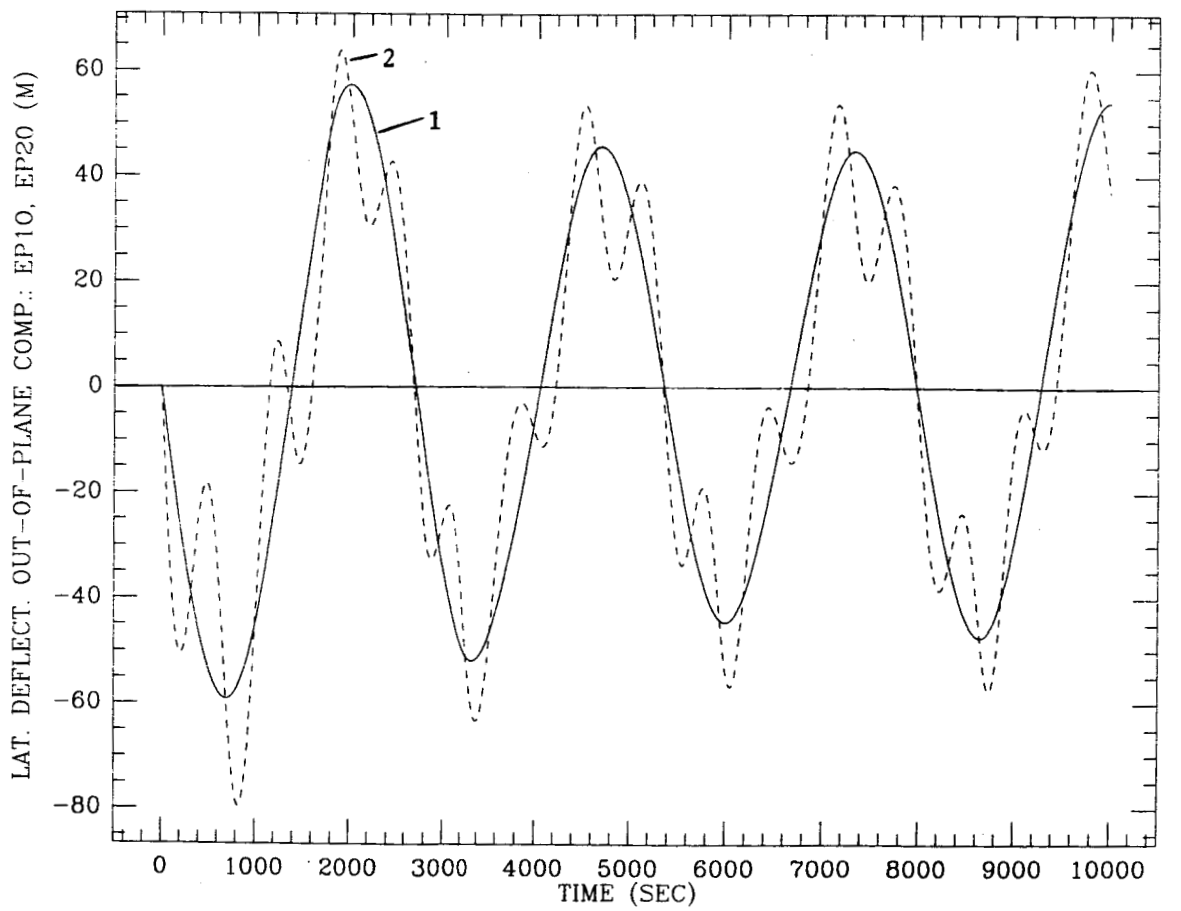

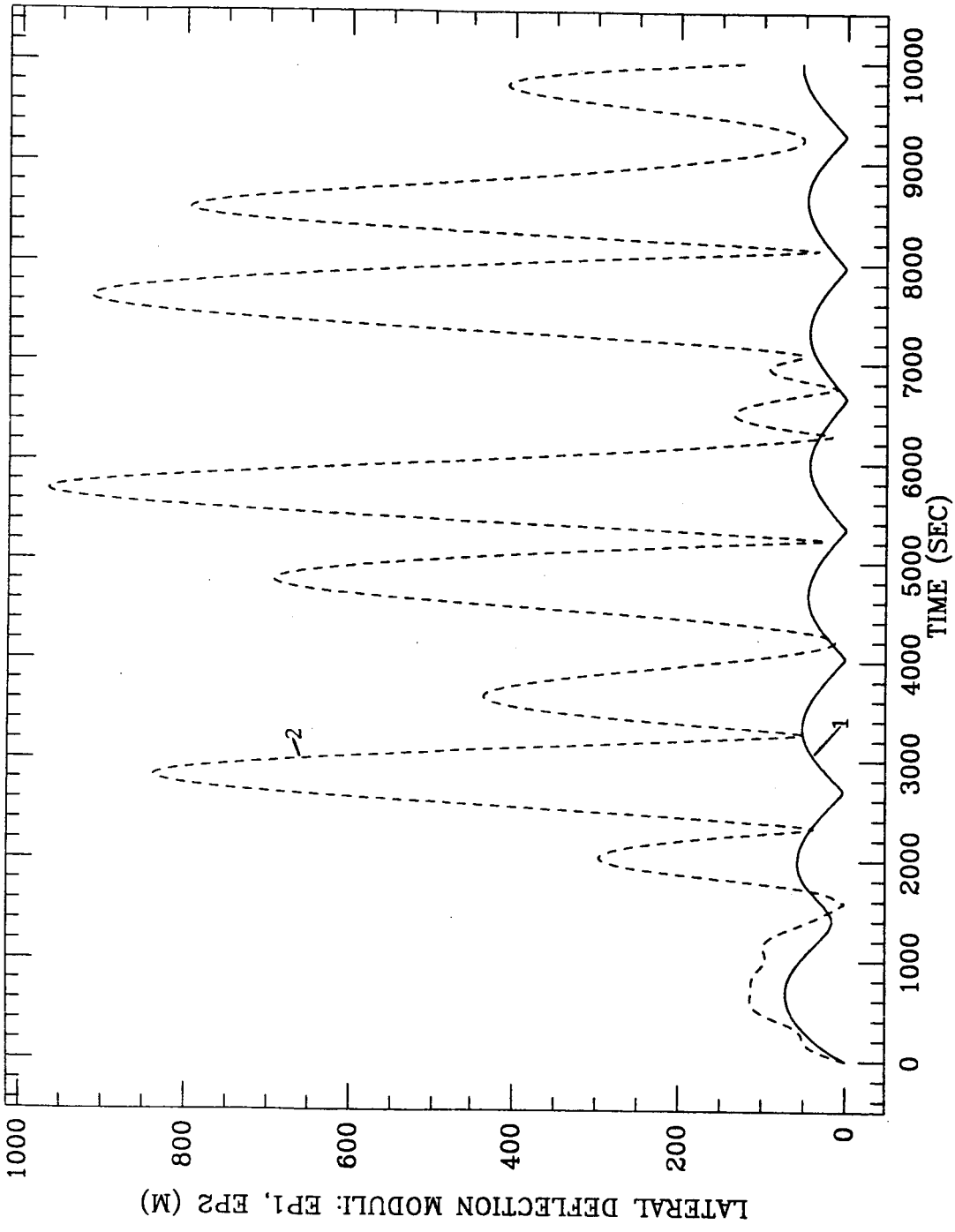
LATERAL DEFLECTION MODULI: EP1, EP2 (M)
1000
800
600
400
200
0
0
1000
2000
3000
4000
5000
6000
7000
8000
9000
10000
TIME (SEC)
1
2

Figure 4i.

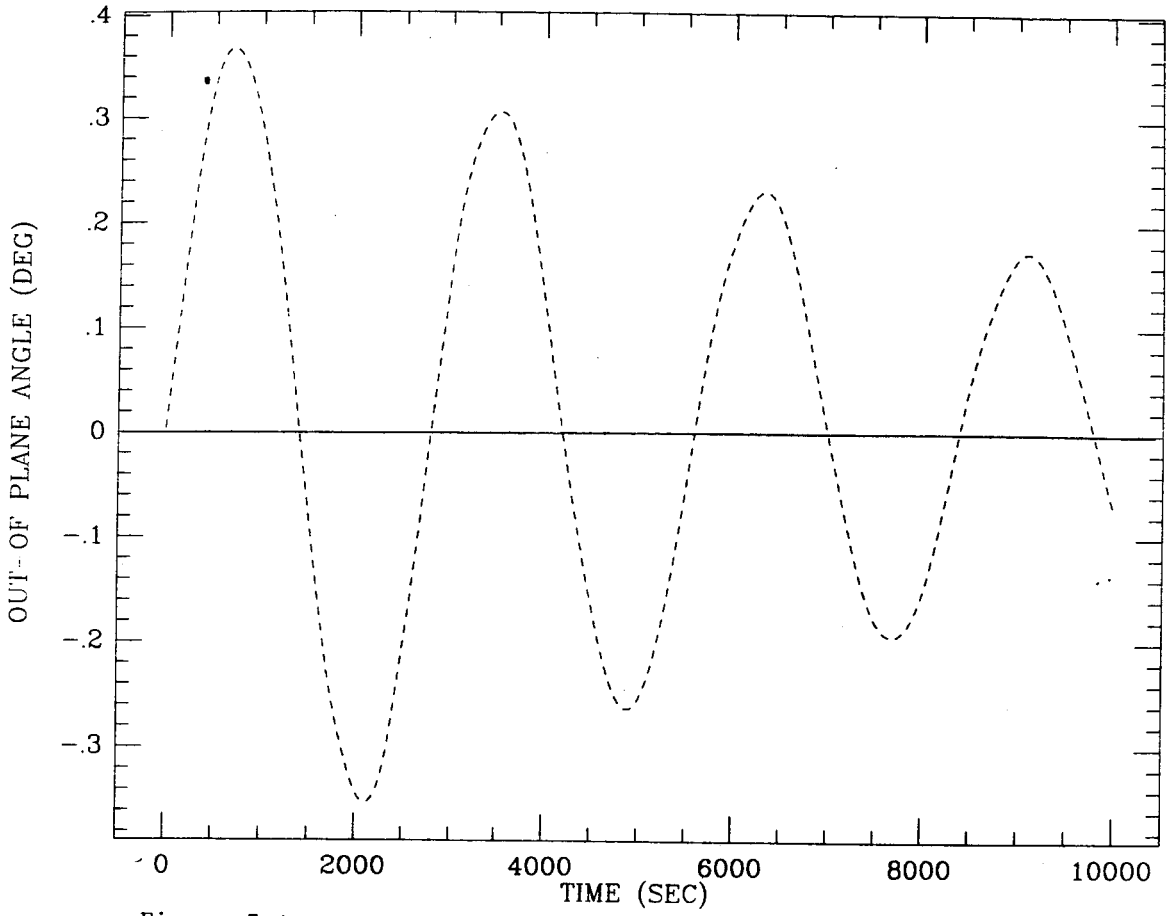

Figure 5a↑

Figure 5b↓

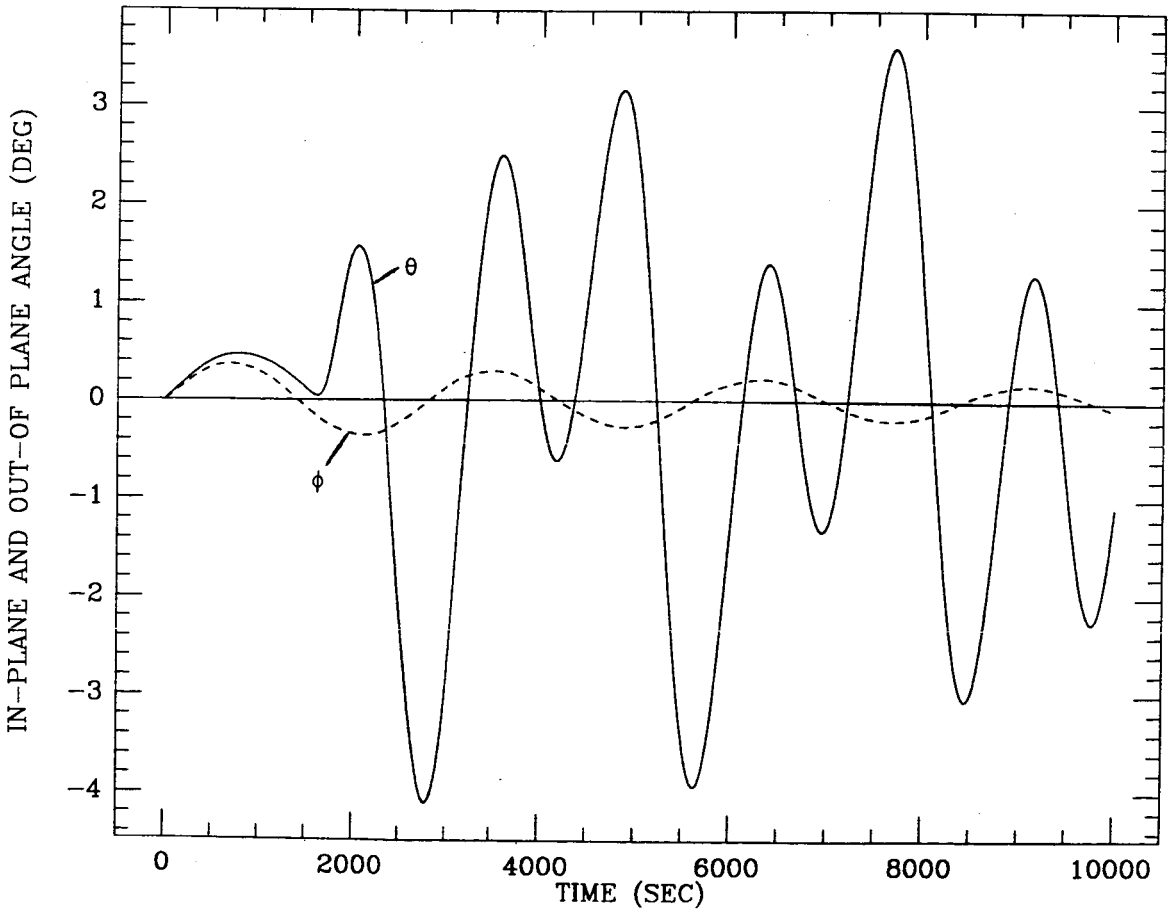

This phenomenon, however, is not very important in the present simulation as it clearly appears from Figure 6b that shows the tether length variation for out-of-plane libration damping (ℓ_{DLOL}) vs. the out-of-plane angle. The phase difference is fairly constant as it can be inferred by the crossing points of the eight-shaped curves close to the φ=0 vertical line. 2) The system is probably settling down to a state in which energy, through exchange among the various degrees of freedom, is flowing into the least damped degrees of freedom. This conclusion can be preliminarily inferred from Figure 6c that shows the angular foot-print of the system (out-of-plane libration vs. in-plane libration). At approximately the same time when the damping starts decreasing the system gets trapped in an eight-shaped angular foot-print.

Figure 6d shows the in-plane angle vs. time along with the out-of-plane angle vs. time. The in-plane angle is clearly forced by the tether length variation for the control of out-of-plane librations. By adopting the standard smooth yo-yo control law, however, the spill-over decreases with time. Figures 6e and 6f are the phase-planes for the φ and θ oscillations respectively. Figures 6g and 6h show the tether length variation per unit tether length for the out-of-plane and in-plane oscillation control respectively. Figure 6i and 6j show the in-plane and out-of-plane components respectively of the lateral deflections of the Space Station (solid line) and the G-laboratory (dotted line). The in-plane component of the lateral deflection of the G-laboratory is excited at the beginning of the simulation by the out-of-plane control spill-over but it decreases as the spill-over decreases. The out-of-plane components of lateral deflections of both the Space Station and the G-laboratory increase slowly with time. Since there is no control over such components in all these simulation runs the energy is probably accumulating in these degrees of freedom. Figures 6k, 6ℓ and 6m depict the tether length variations for tether no. 1, no.

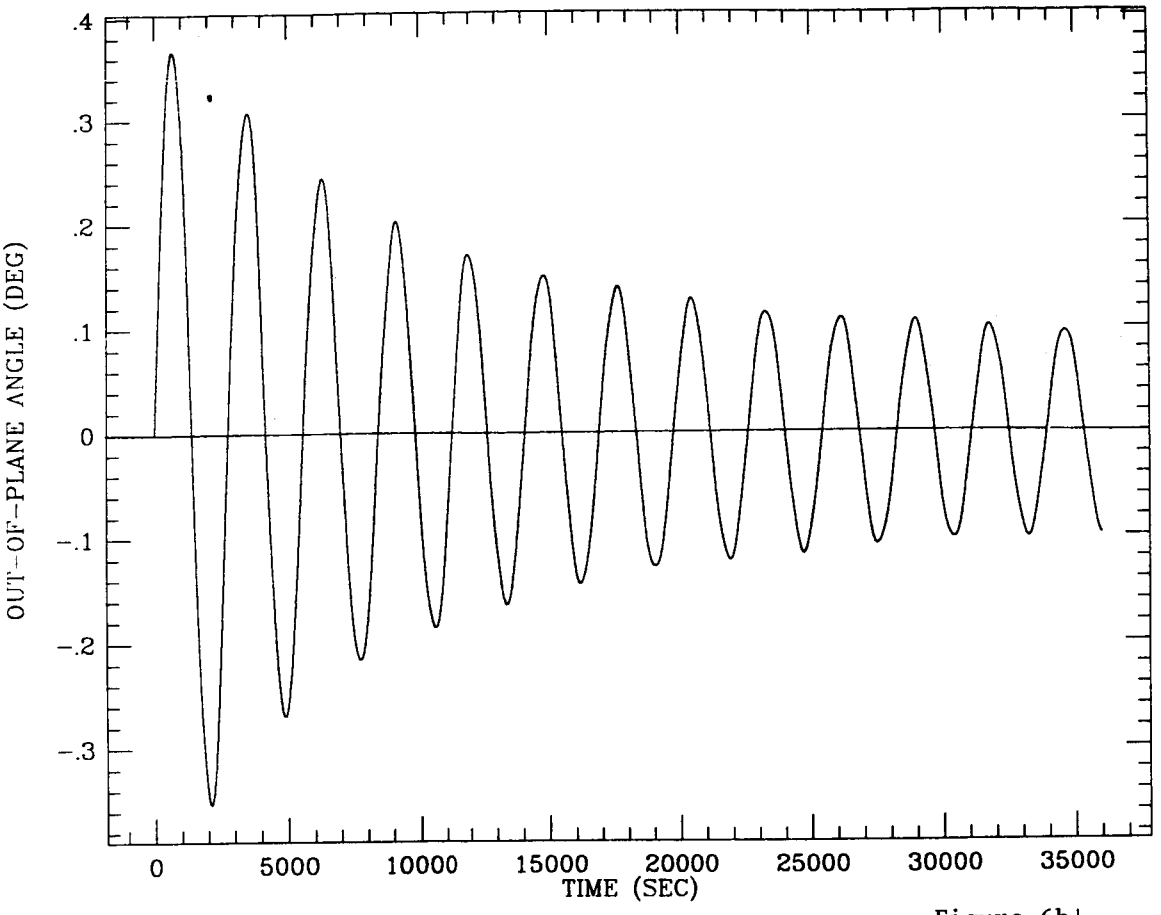

Figure 6a↑

Figure 6b↓

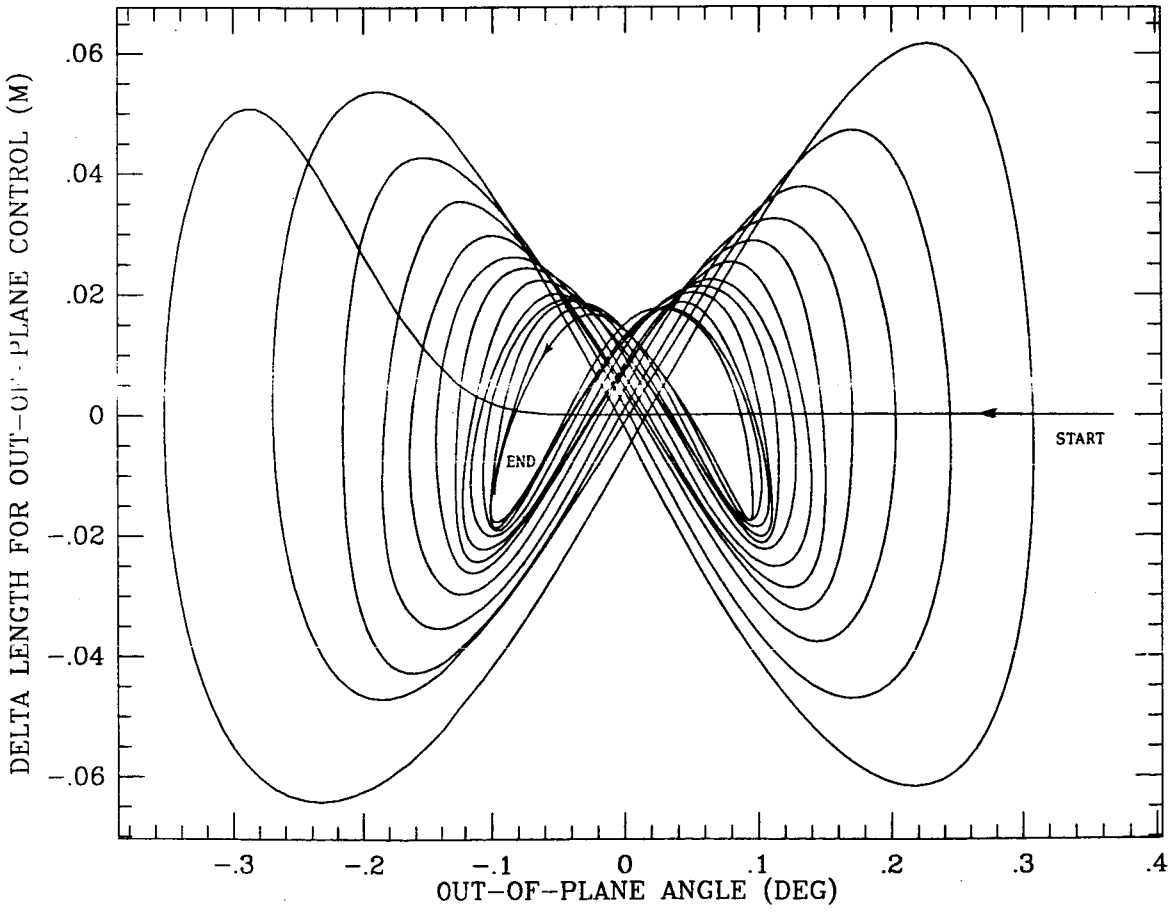

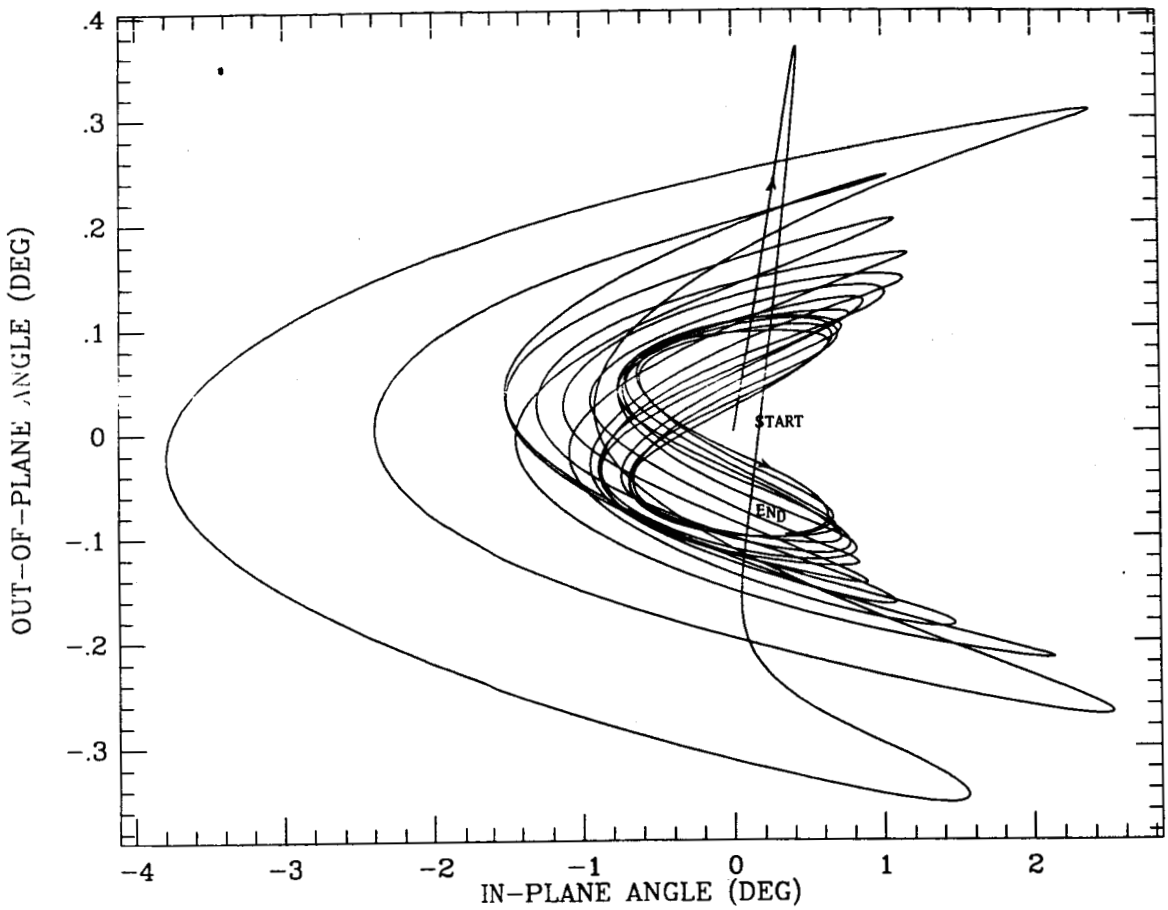

Figure 6c↑

Figure 6d↓

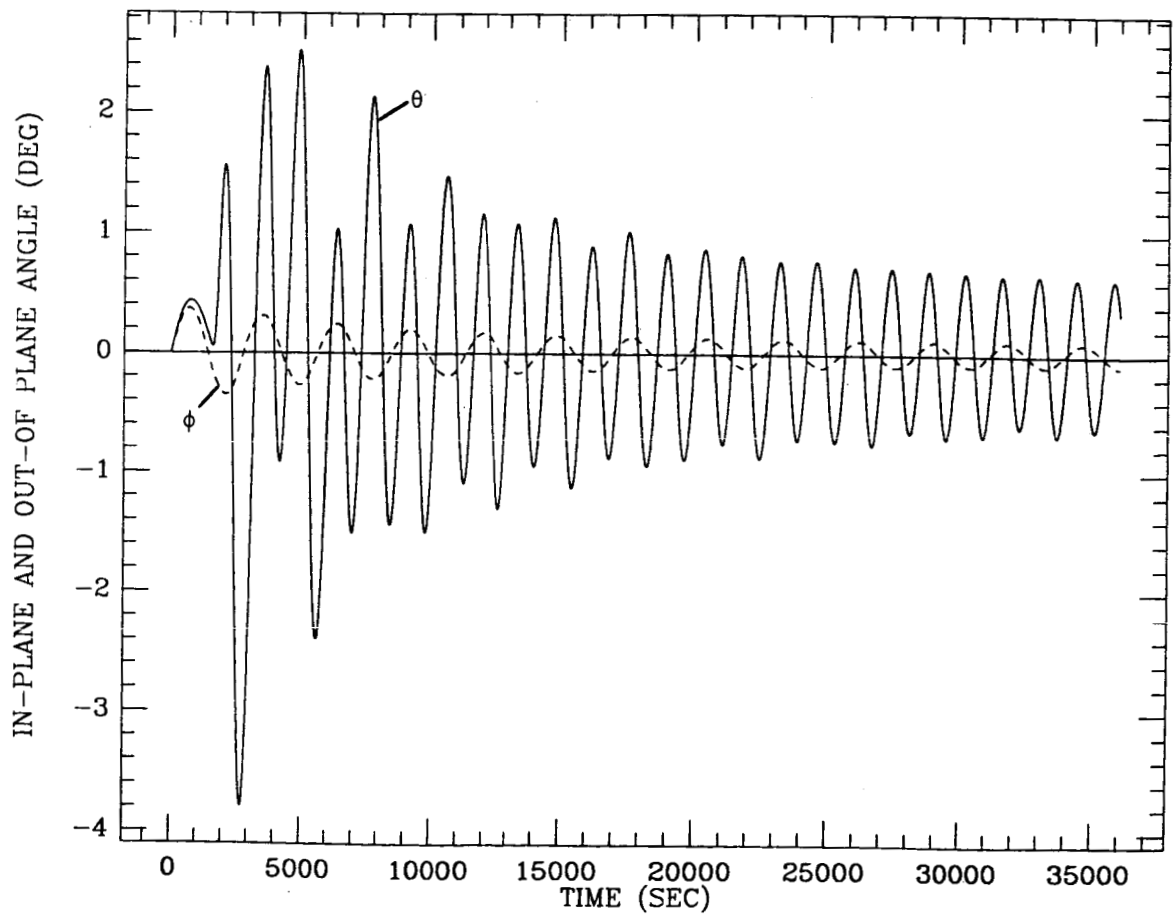

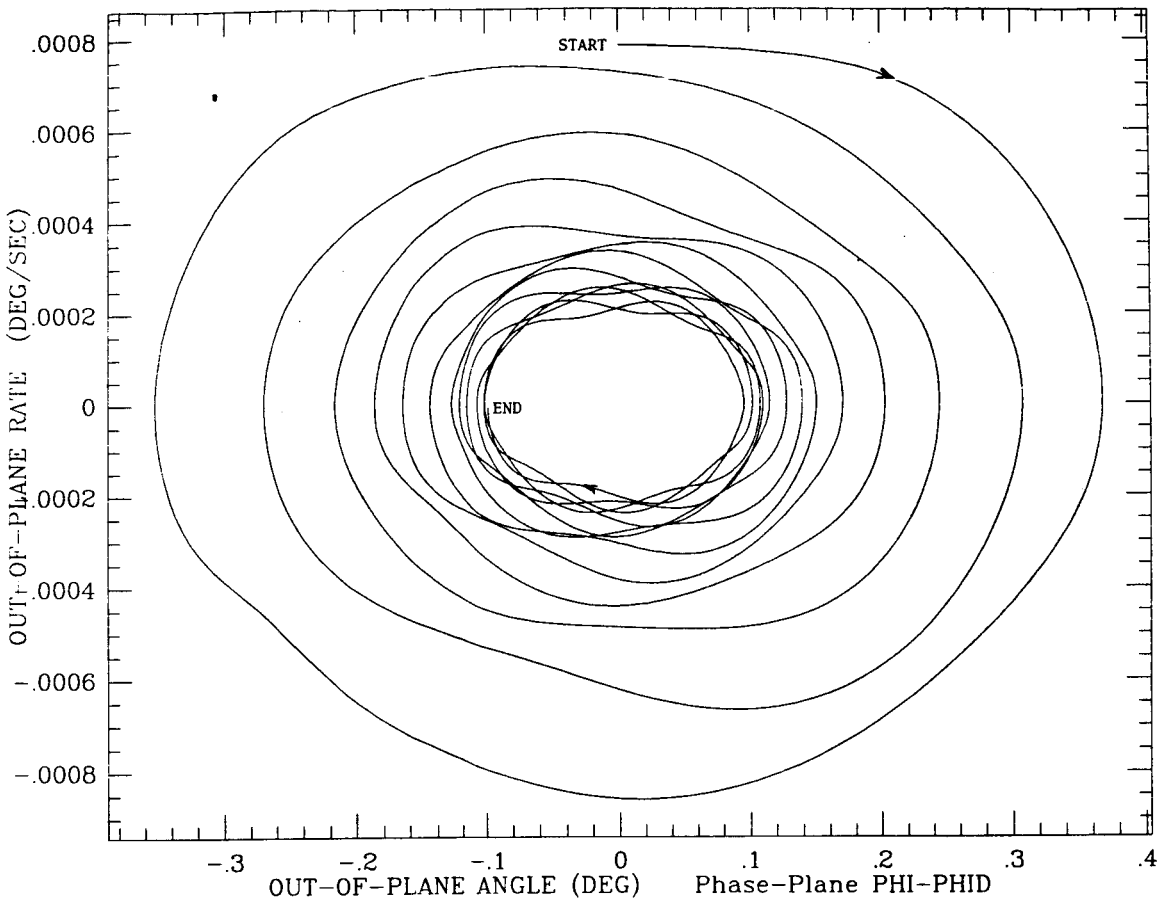

Figure 6e↑

Figure 6f↓

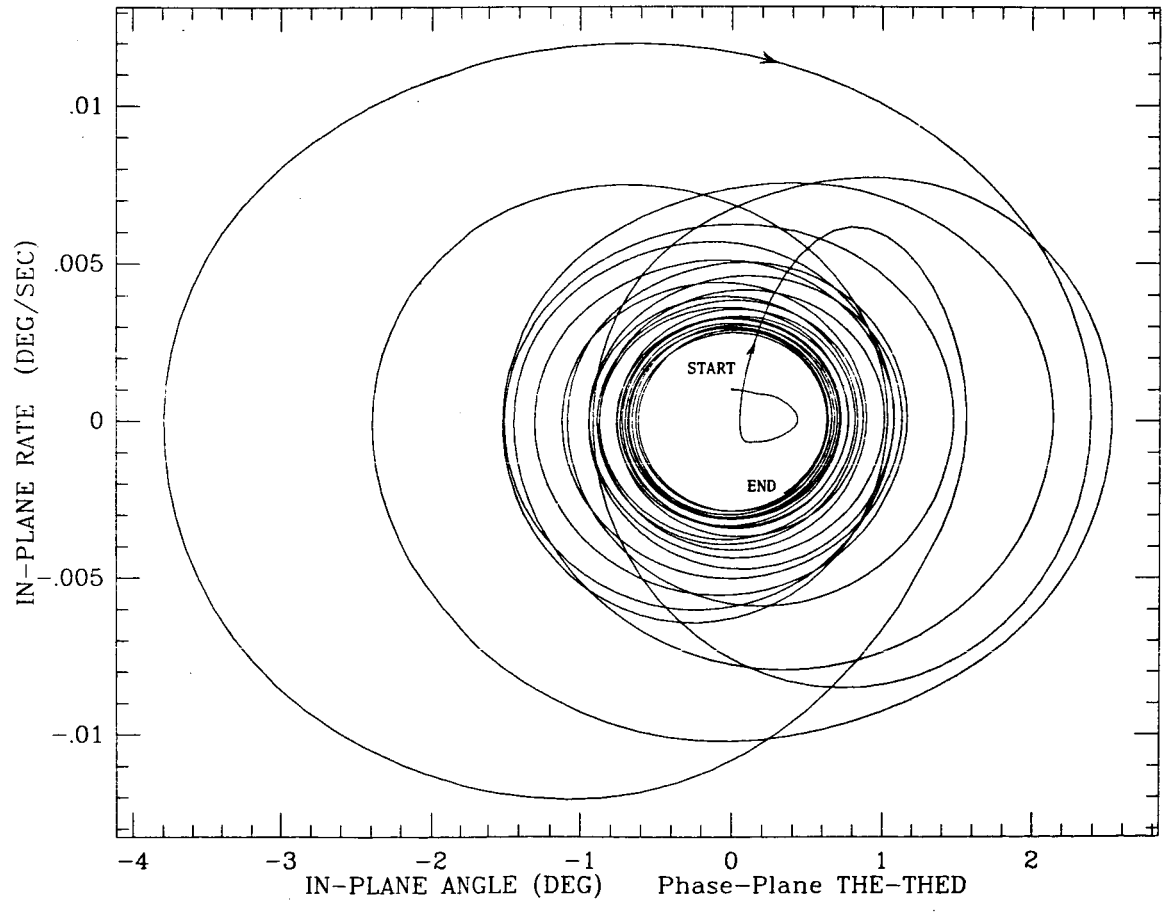

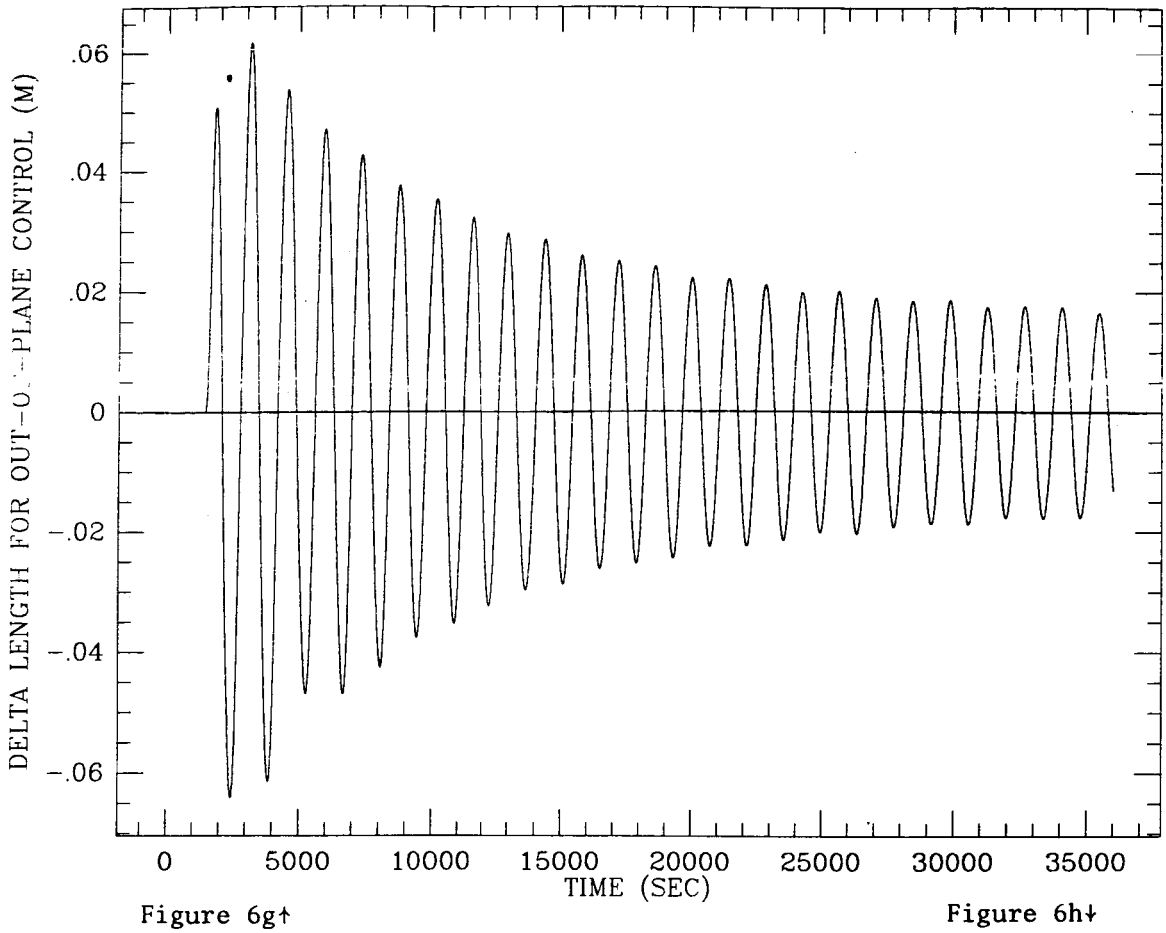

Figure 6g↑

Figure 6h↓

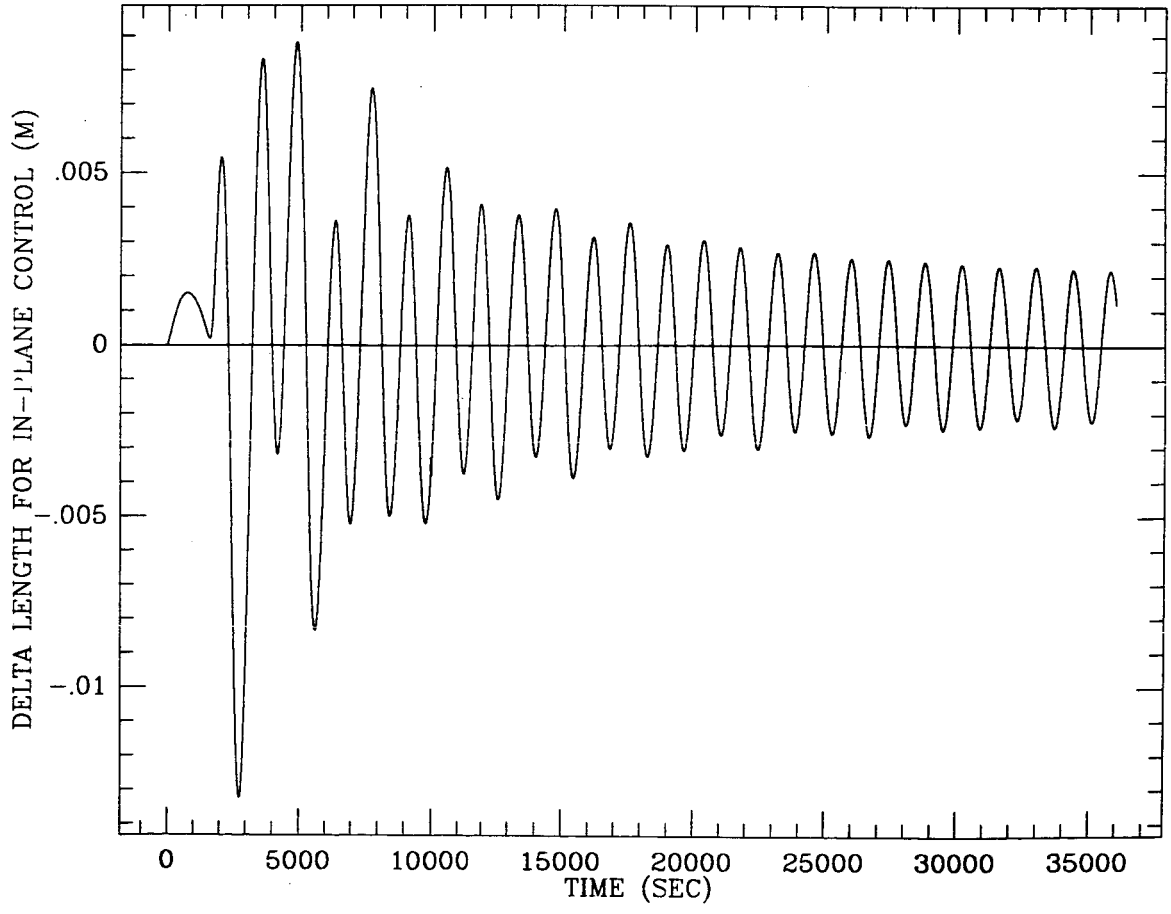

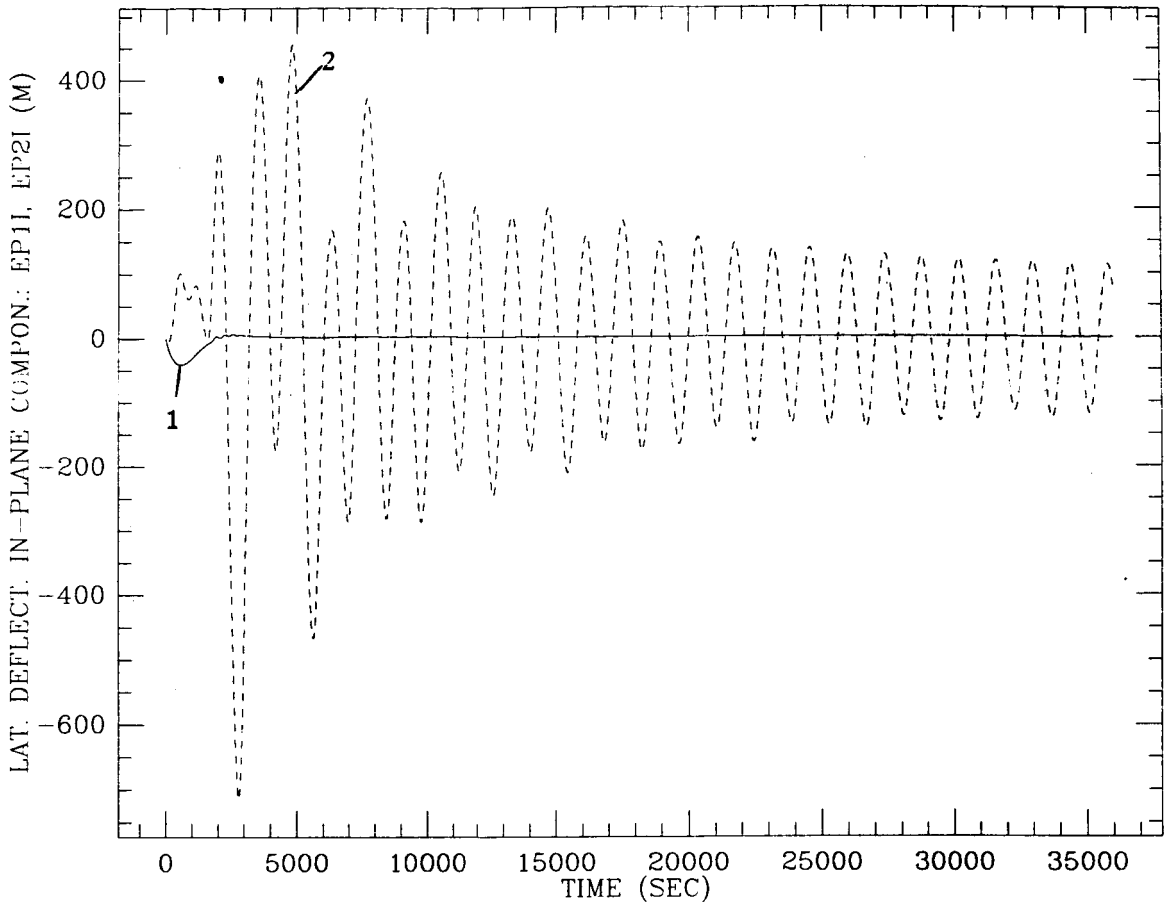

Figure 6i↑

Figure 6j↓

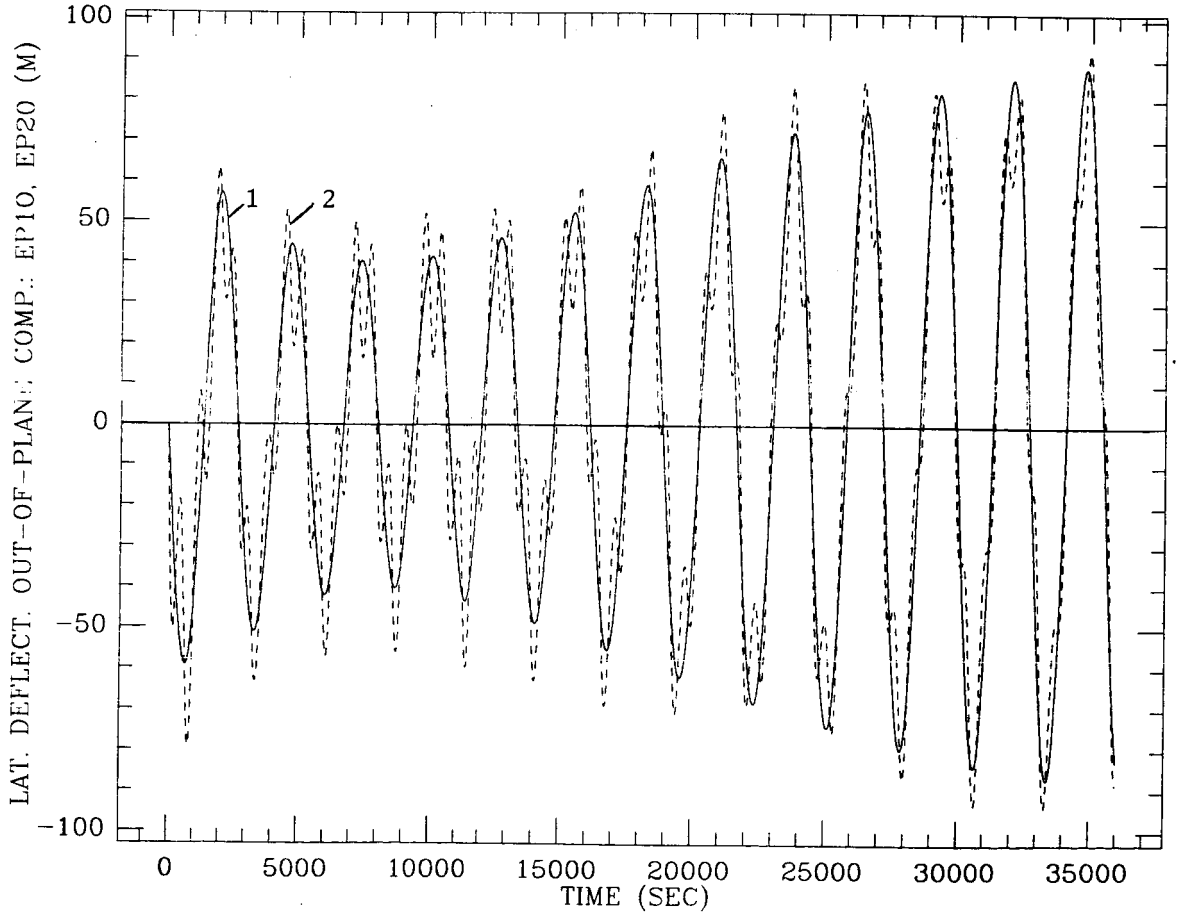

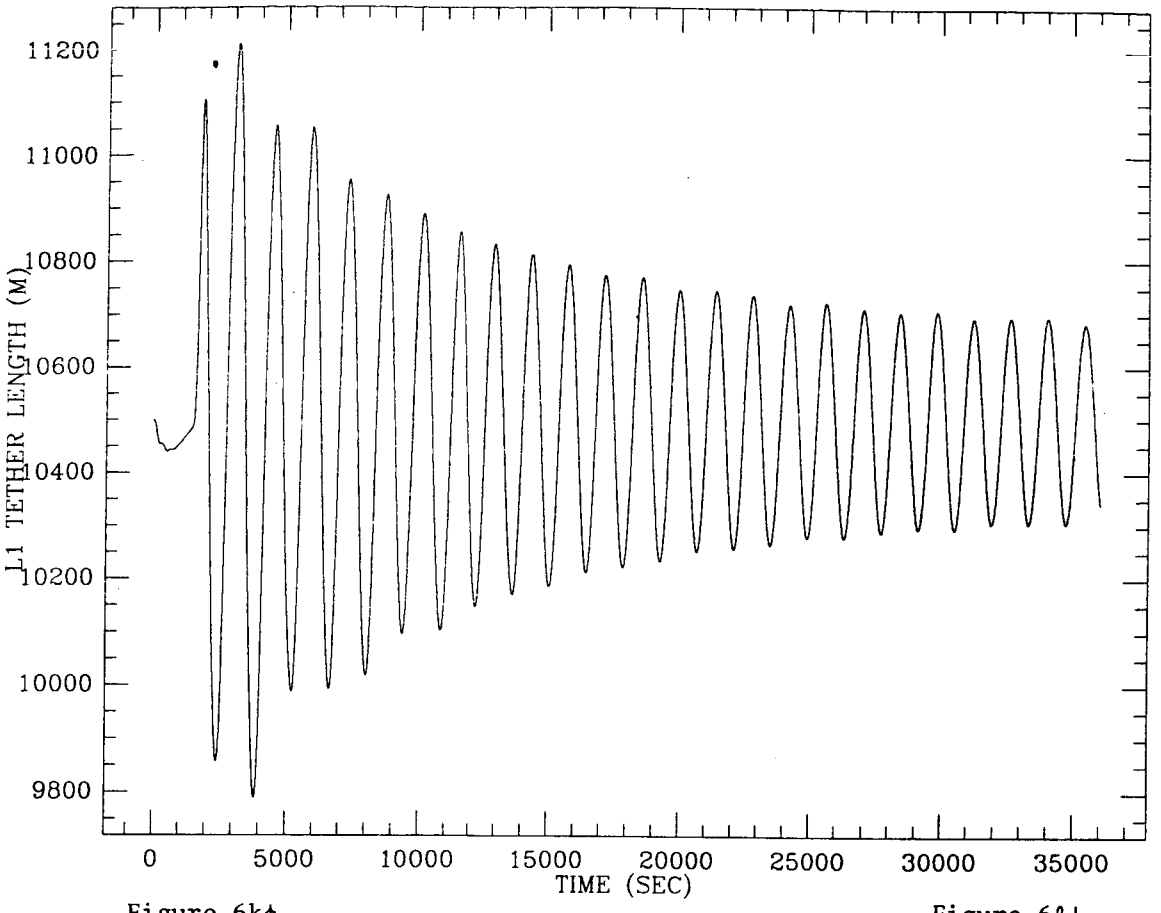

Figure 6k↑

Figure 6ℓ↓

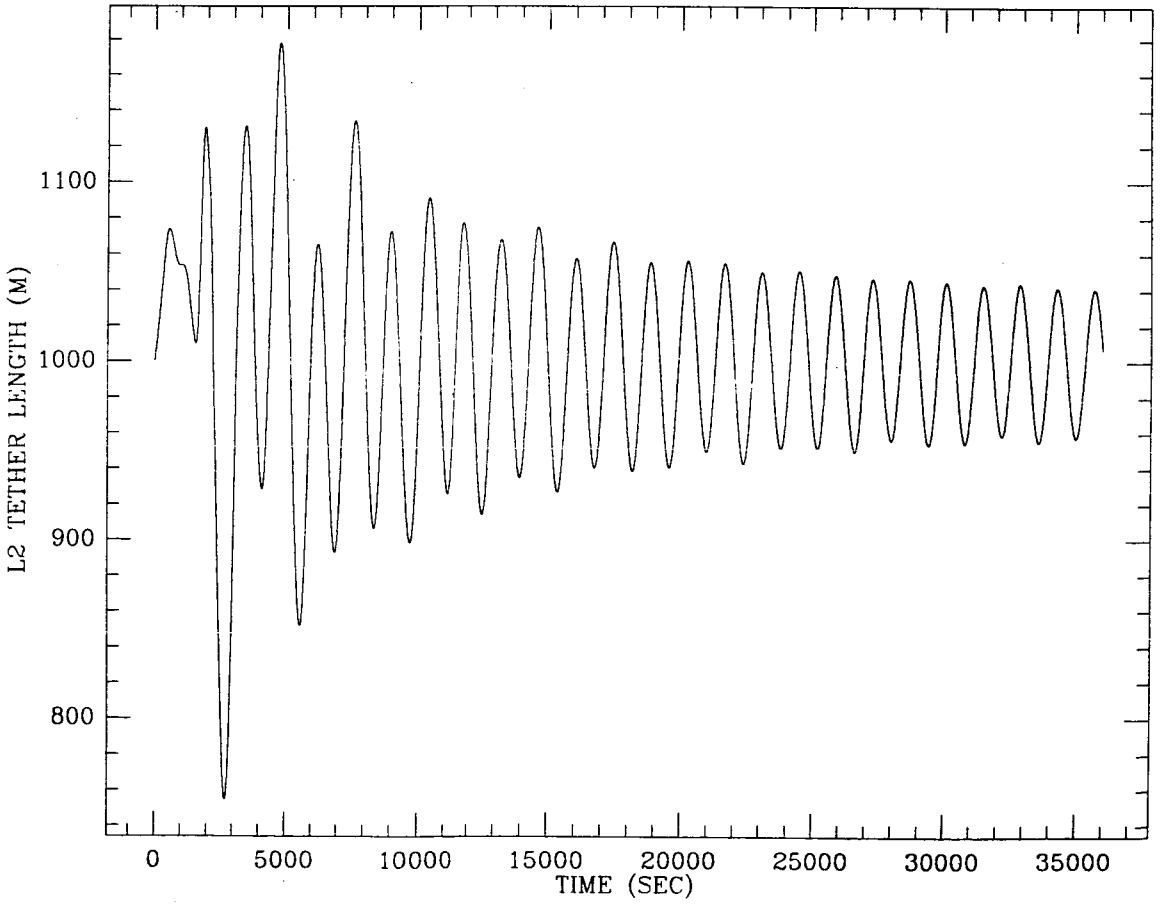

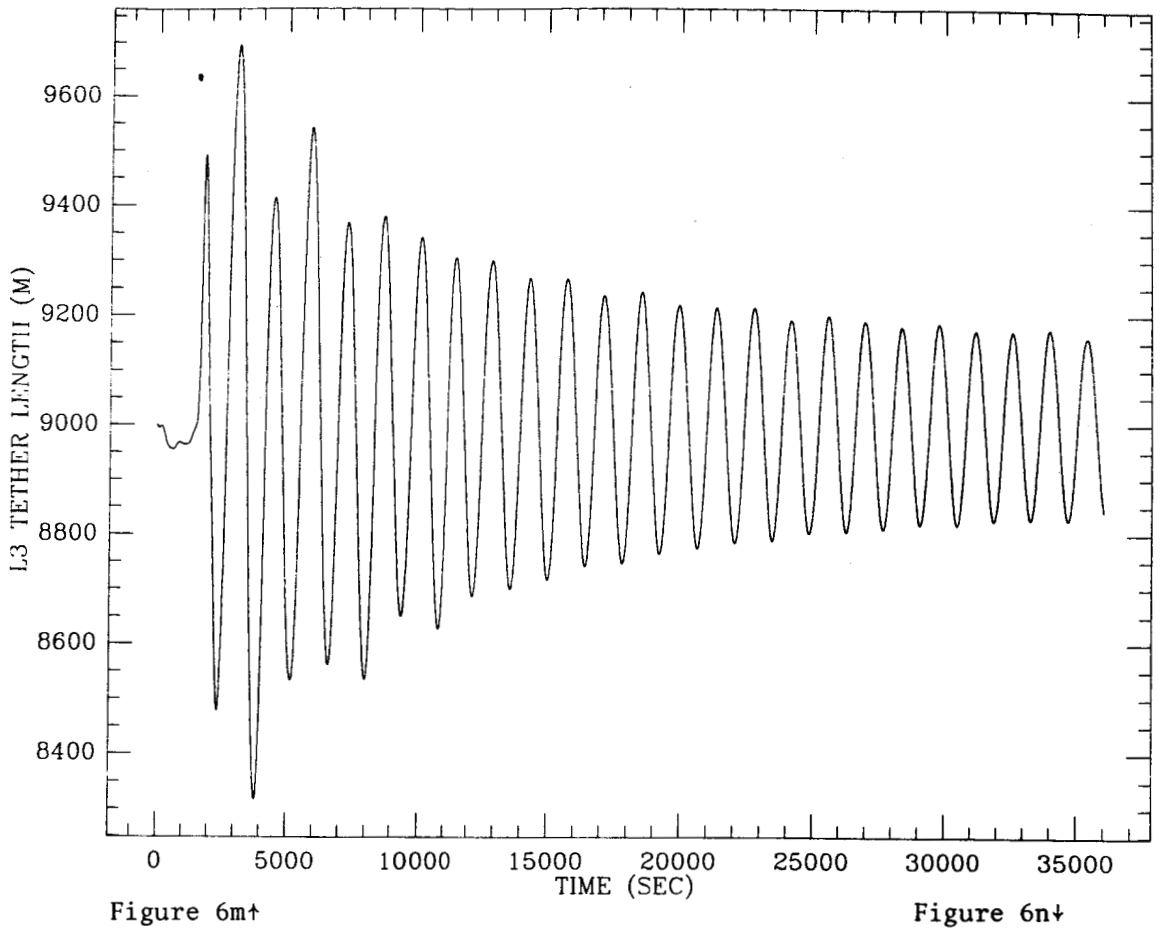

Figure 6m↑

Figure 6n↓

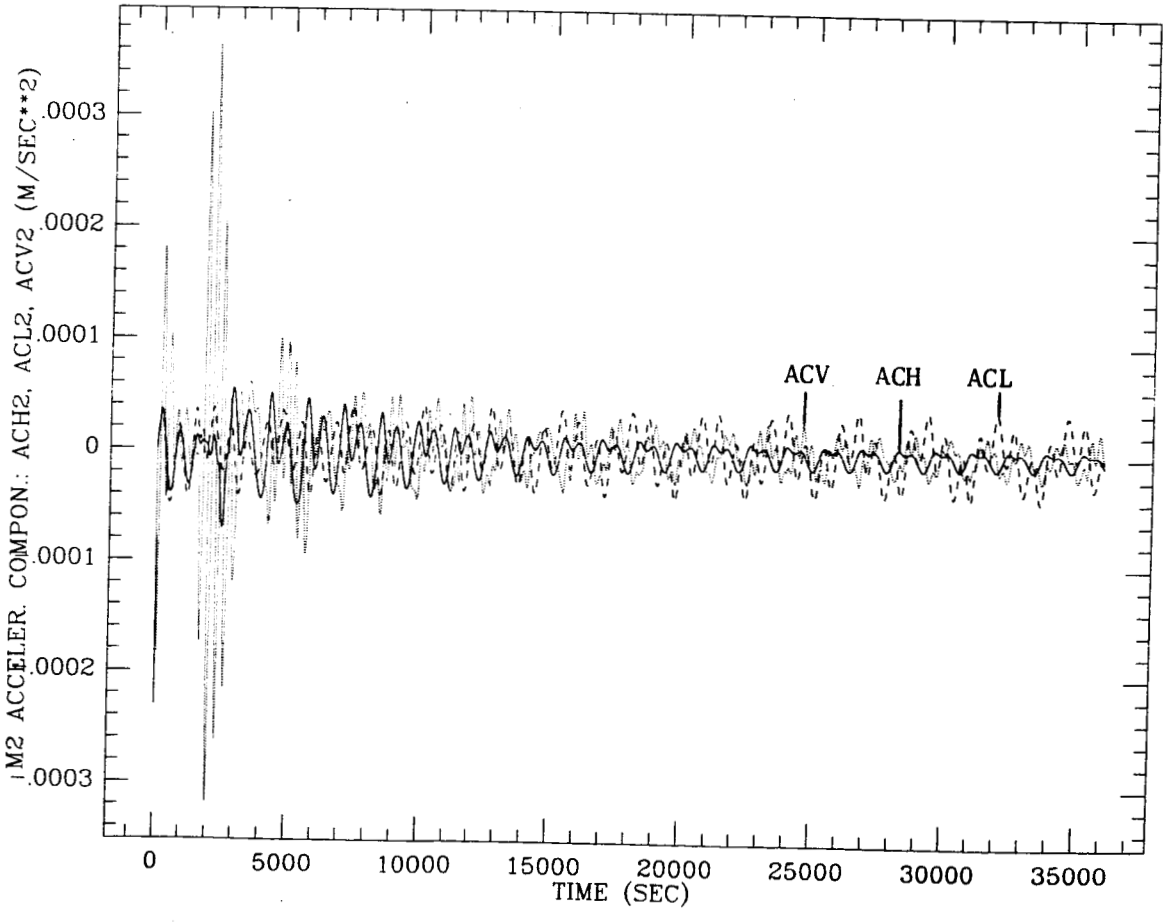

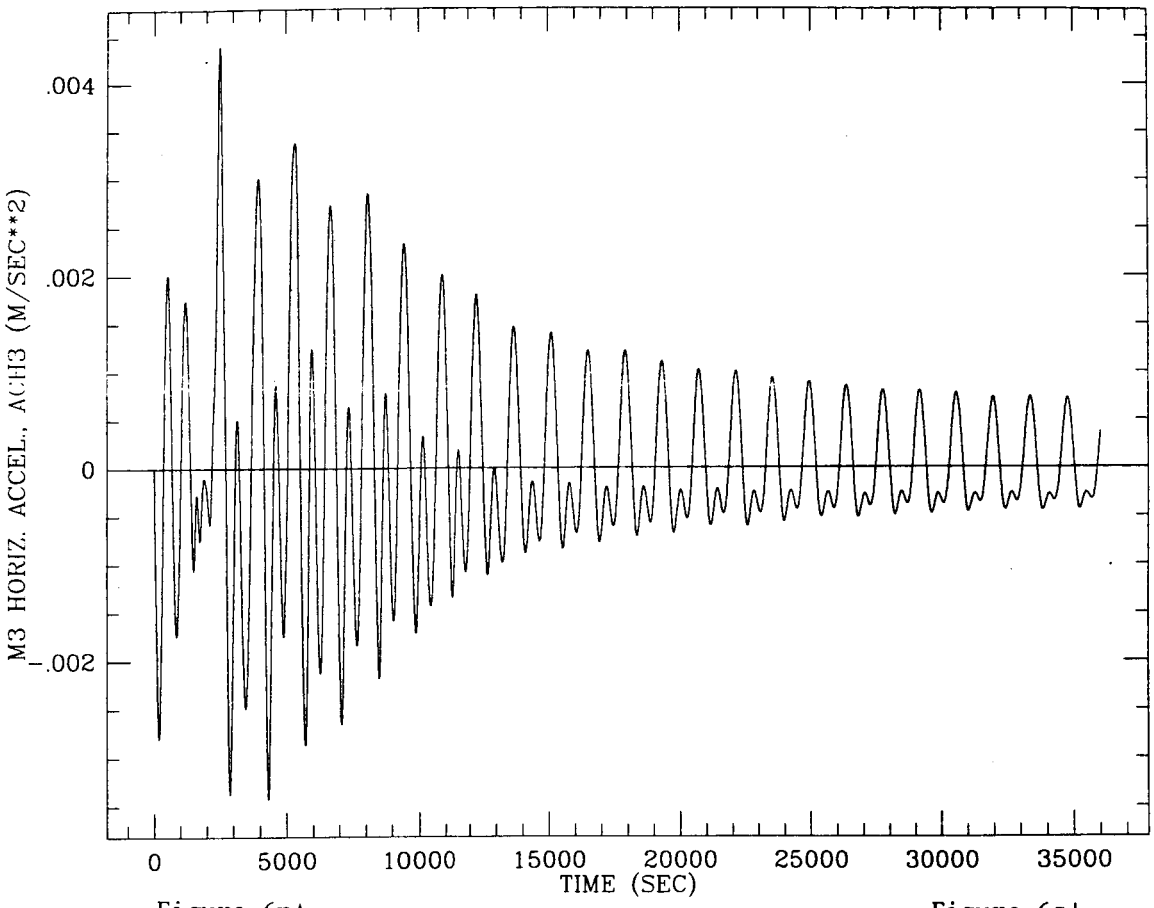

Figure 6p↑

Figure 6q↓

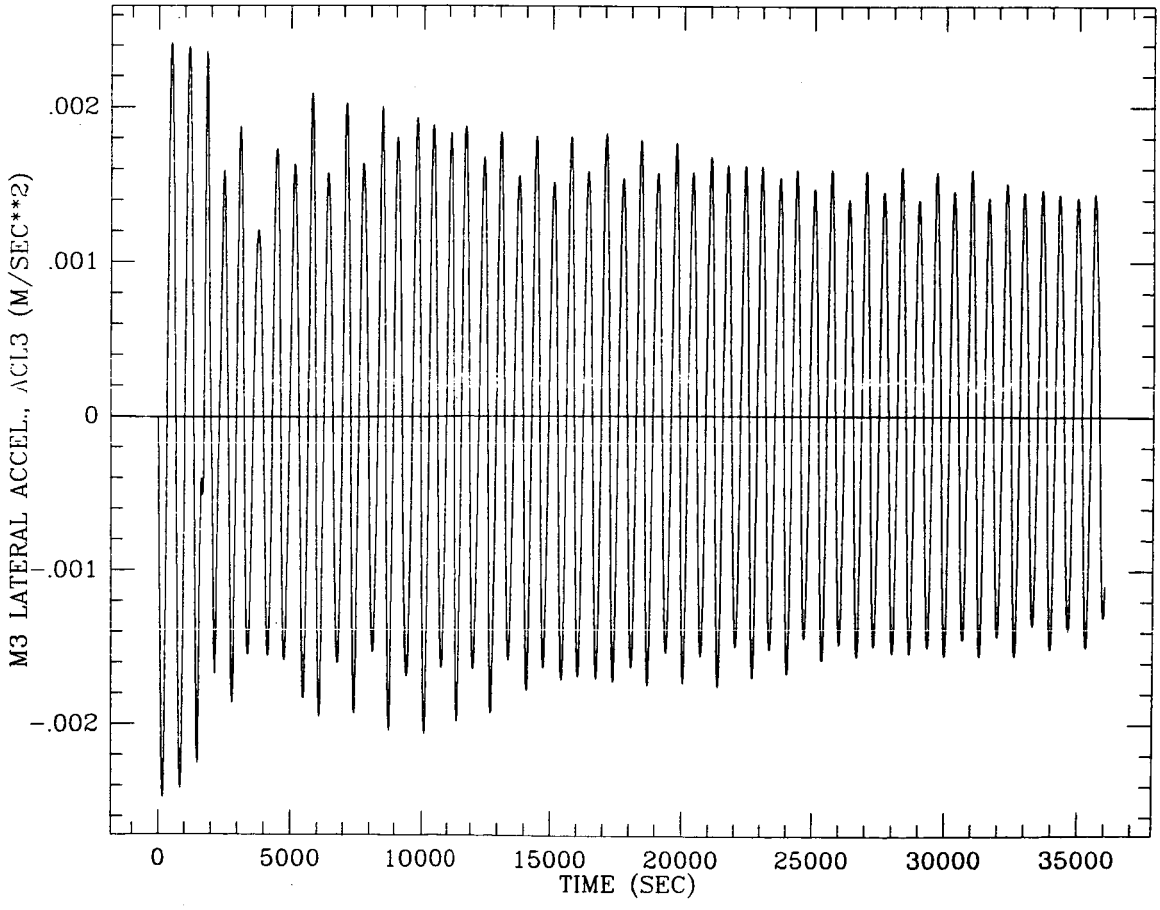

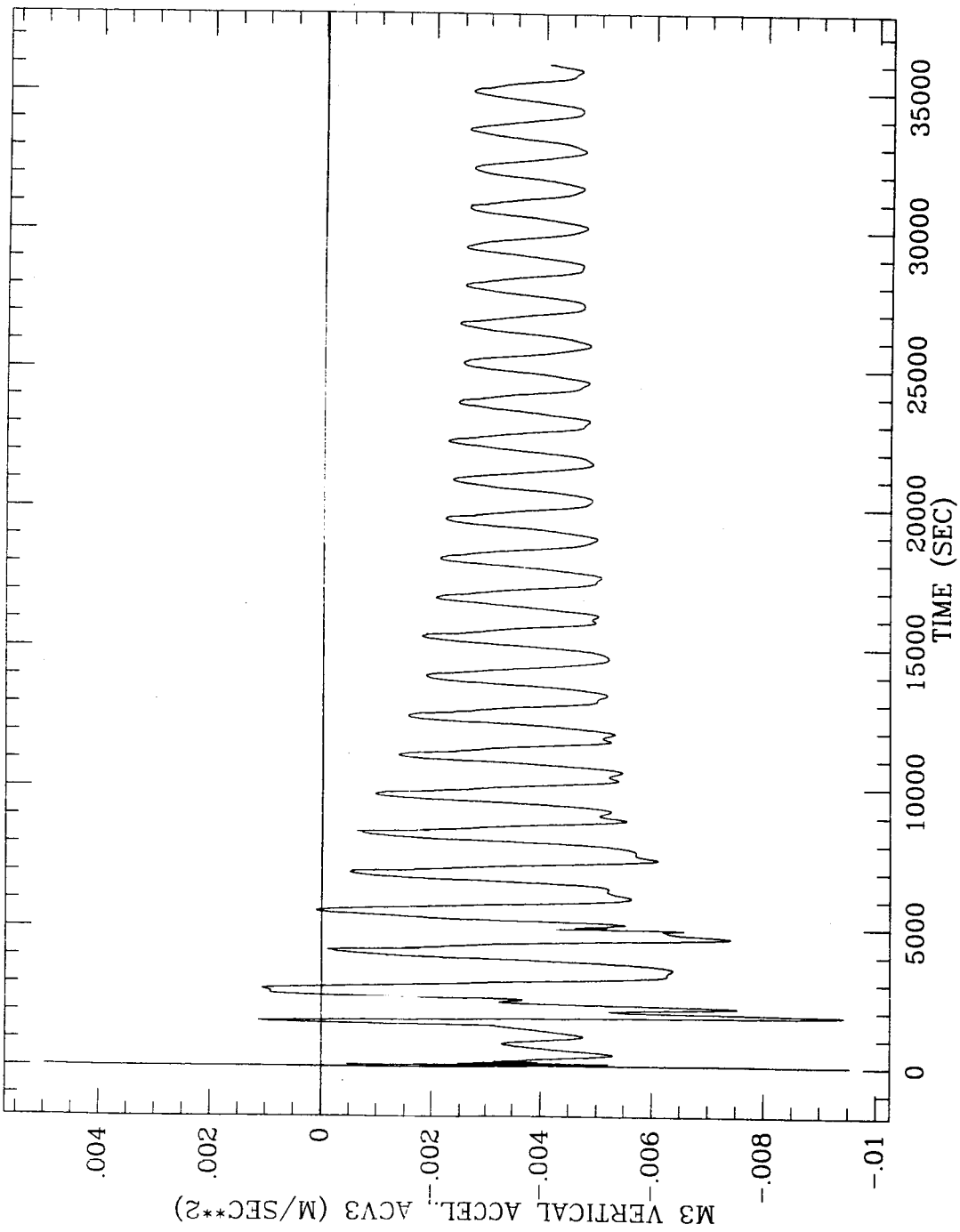
M3 VERTICAL ACCEL. ACV3 (M/SEC**2)
.004
.002
0
-.002
-.004
-.006
-.008
-.01
0
5000
10000
15000
20000
25000
30000
35000
TIME (SEC)

Figure 6r.

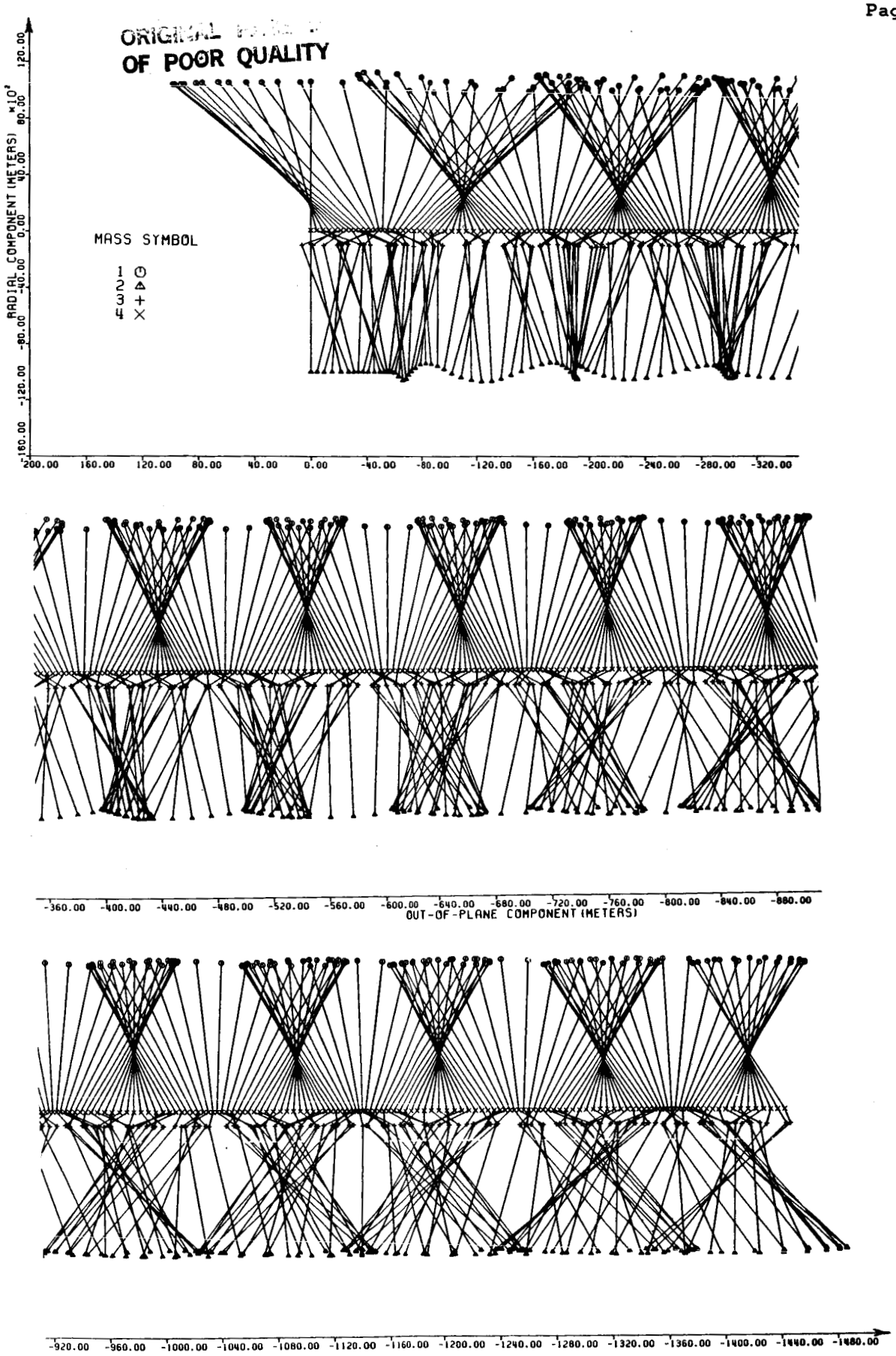

Figure 7a. Front-view. Snapshots every 100 sec for 36,000 sec.

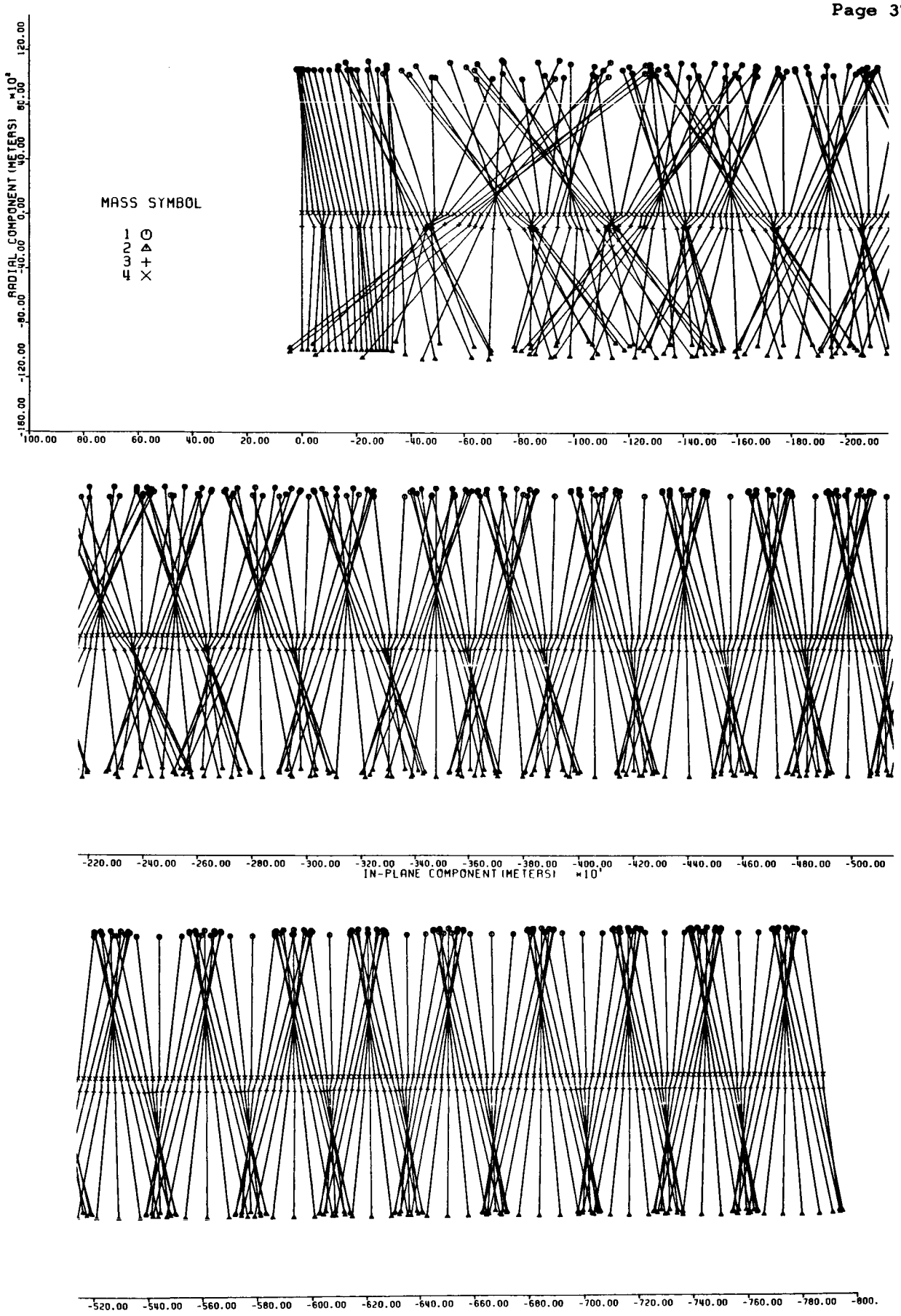

Figure 7b. Side-view. Snapshots every 100 sec for 36,000 sec.

2 and no. 3 respectively. In order to give an idea of the acceleration fluctuations during the out-of-plane damping process Figure 6ℓ depicts the three components, in the orbiting reference frame, of the acceleration on board the Space Station. The residual acceleration is due to the fact that all the initial oscillations have not been damped out completely. The in-plane libration however can be damped out very effectively by disactivating the out-of-plane yo-yo control and by increasing the gain of the in-plane control system. The following figures, therefore, should not be interpreted as the limit performance of the system. Figures 6p, 6q and 6r show the flight direction (ACH), transverse (ACL) and vertical (ACH) component of the acceleration on board the G-laboratory vs. time. Because of the relatively large residual libration amplitudes the residual acceleration fluctuations on board the G-laboratory are larger than the acceleration fluctuations on board the Space Station. Finally Figures 7a and 7b show the expanded-scale (the expansion coefficient is different for the two figures) front-view and side-view respectively of the system with snapshots every 100 sec up to 36,000 sec. The residual oscillations of the system are clearly evident in these two figures.

2.3 Environmental Models

We have developed an entirely new package of subroutines which model the environment at the altitudes of interest to the Space Station.

We have modeled the major perturbations acting upon a tethered system in the range of altitudes from 400 km to 600 km. The major perturbations are: drag, J_2 gravity term and thermal as dealt with in detail in the next subsections.

2.3.1 Drag Model -

As a density model we have adopted the version by C.E. Roberts Jr., reference [1], who developed an analytical model of upper atmosphere which provides atmospheric density as a function of exospheric temperature and altitude. The model is based on Jacchia's 1970, taking also into account the '77 corrections [2]. The temperature equation has been modified in order to have a simple analytical expression of the temperature as a function of the height h.

The atmospheric density is given by:

$$\rho(h) = \sum_{i=1}^{6} M_i d_i(h) \qquad (2.3.1)$$

where:

i = constituents = N_2, Ar, He, O_2, O, H

M_i = molecular mass (gr/mole)

d_i = number of particles of each constituent per cm^3/Avogadro's number

$$d_i(h) = d_i(h_{125}) \left(\frac{T_x}{T(h)}\right)^{1+\alpha_i+\gamma_i} \left(\frac{T_{EX} - T(h)}{T_{EX} - T_x}\right)^{\gamma_i} \qquad (2.3.2)$$

$d_i(h_{125})$ = computed data at h = 125 km

T_{EX} = exospheric temperature

α_i = thermal diffusion coefficients

T_x = f(exospheric temperature) = $A_1 + A_2 T_{EX} + A_3 \exp(A_4 T_{EX})$

$$T(h) = T_{EX} - (T_{EX} - T_x) \exp\left[-\left(\frac{T_{EX} - T_0}{T_{EX} - T_x}\right)\left(\frac{h - h_x}{h_x - h_0}\right)\left(\frac{\ell}{R_e + h}\right)\right] \qquad (2.3.3)$$

T_o = 188 °K

h_x = 125 km

h_o = 90 km

ℓ = to be chosen in order to produce a minimum in the absolute value of the percentage difference with the Jacchia's model for altitudes between 125 and 1000 km and for T_{EX} between 600°K and 2000°K

R_a = effective earth's radius = 6356.766 km

$$\gamma_i = \frac{M_i g_o R_a^2}{R \ell T_{EX}} \left(\frac{T_{EX} - T_x}{T_{EX} - T_0}\right)\left(\frac{h_x - h_0}{R_a + h_x}\right) \qquad (2.3.4)$$

g_o = gravity acceleration on the ground = 9.80665 $\frac{m}{s^2}$

R = universal gas constant = 8.31432 J/°K-mole

The number of particles of atomic hydrogen d_H is equal to zero for h < 500 km. As a result of the above mentioned computations Figure 8 shows the atmospheric density vs. altitude, in the range of interest to our system, for different exospheric temperatures.

In order to obtain a more accurate density model we have improved the "static model" by taking into account the phenomena which affect the values of the global exospheric temperature [3]. We have modeled the effects of solar activity and diurnal variations but we have neglected the geomagnetic activity. Following these assumptions we can express the local exospheric temperature T_L as follows:

$$T_L = T_c(1 + R_T \sin^m\theta)\left(1 + R_T \frac{\cos^m\eta - \sin^m\theta}{1 + R_T \sin^m\theta} \cos^n \frac{\tau}{2}\right) \qquad (2.3.5)$$

where:

T_c = night minimum of the global exospheric temperature, function of solar activity

R_T = cost = .3 = amplitude of temperature variation

m = cost = 2.2

n = cost = 3.0

θ = $|\phi + \delta_\odot|/2$

η = $|\phi - \delta_\odot|/2$

τ = $|H + \beta + p \sin (H+\gamma)|$

ϕ = latitude of the satellite

$\delta_\odot$ = declination of the sun

H = hour angle of the sun

β = lag of the temperature maximum with respect to the sun's culmination = cost = -37°

τ = asymmetry of temperature distribution = cost = +6°

γ = location of temperature distribution asymmetry = cost = +43°

Figures 9a, 9b, 9c and 9d show the density and the local exospheric temperature variations vs. time (1 orbit) in two different seasonal situations: Spring equinox and Summer solstice.

The deceleration of the i^{th}-mass m_i due to drag is given by:

$$\vec{F}_{d,i} = -\beta_i \rho_i |V_i| \vec{V}_i \qquad (2.3.6)$$

where:

β_i = ballistic coefficient of the i^{th}-mass $= \frac{C_{D,i} A_i}{2m_i}$

A_i = cross section of the i^{th}-mass

$C_{D,i}$ = drag coefficient of the i^{th}-mass

ρ_i = $\rho(h_i)$ = atmospheric density at height h_i

h_i = height of the i^{th}-mass $= R_i - R_\oplus (1 - f\sin^2\lambda_i)$

f = flattening factor of the Earth

$\vec{V}_i$ = velocity of the i^{th}-mass relative to the atmosphere

λ_i = latitude of the i^{th}-mass

$R_\oplus$ = earth's equatorial radius

We assume that the atmosphere rotates rigidly with the Earth and, differently

from other authors, we take into account the relative motion between the orbiting frame and the i^{th}-mass m_i. The relative velocity is therefore given by:

$$\vec{V}_i = \dot{\vec{R}}_i - \vec{\Omega}_\oplus \times \vec{R}_i \qquad (2.3.7)$$

where $\Omega_\oplus$ is the Earth's angular velocity while R_i is the radius vector from the Earth's center to the i^{th}-mass. We have

$$\begin{aligned} \vec{R}_i &= \vec{R}_o + \vec{r}_i \\ \dot{\vec{R}}_i &= \dot{\vec{r}}_i + \vec{\Omega} \times \vec{R}_i \end{aligned} \qquad (2.3.8)$$

where R_o is the radius vector of the origin of the orbiting reference frame, r_i is the radius vector from that origin to the i^{th}-mass and Ω is the orbital rate. Hence

$$\vec{V}_i = (\vec{\Omega} - \vec{\Omega}_\oplus) \times (\vec{R}_o + \vec{r}_i) + \dot{\vec{r}}_i \qquad (2.3.9)$$

The aerodynamic forces (per unit mass) are readily computed by substituting equation (2.3.9) into equation (2.3.6).

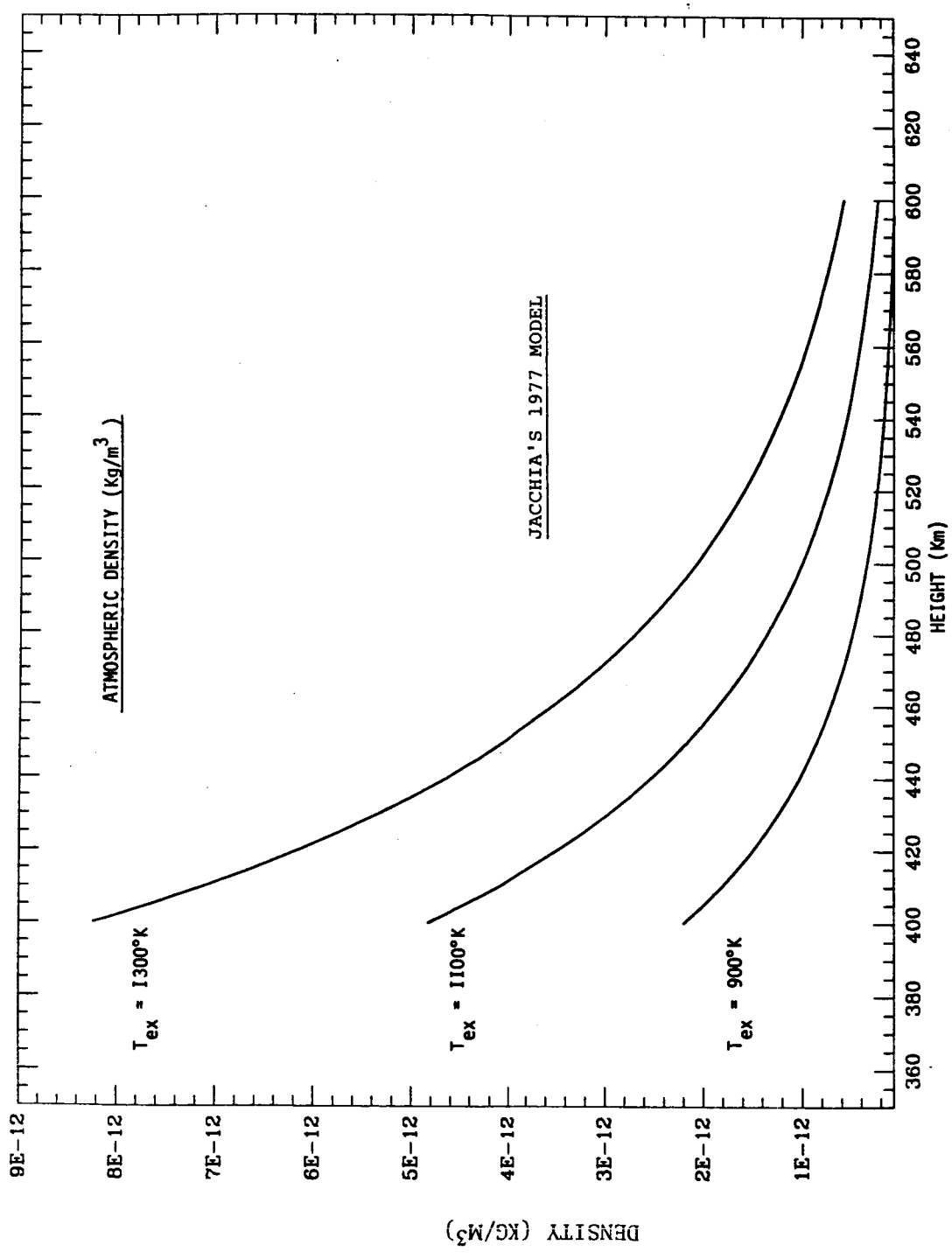
ATMOSPHERIC DENSITY (Kg/m^3)
JACCHIA'S 1977 MODEL
T_{ex} = 1300°K
T_{ex} = 1100°K
T_{ex} = 900°K
9E-12
8E-12
7E-12
6E-12
5E-12
4E-12
3E-12
2E-12
1E-12
360
380
400
420
440
460
480
500
520
540
560
580
600
620
640
HEIGHT (Km)
DENSITY (KG/M3)

Figure 8.

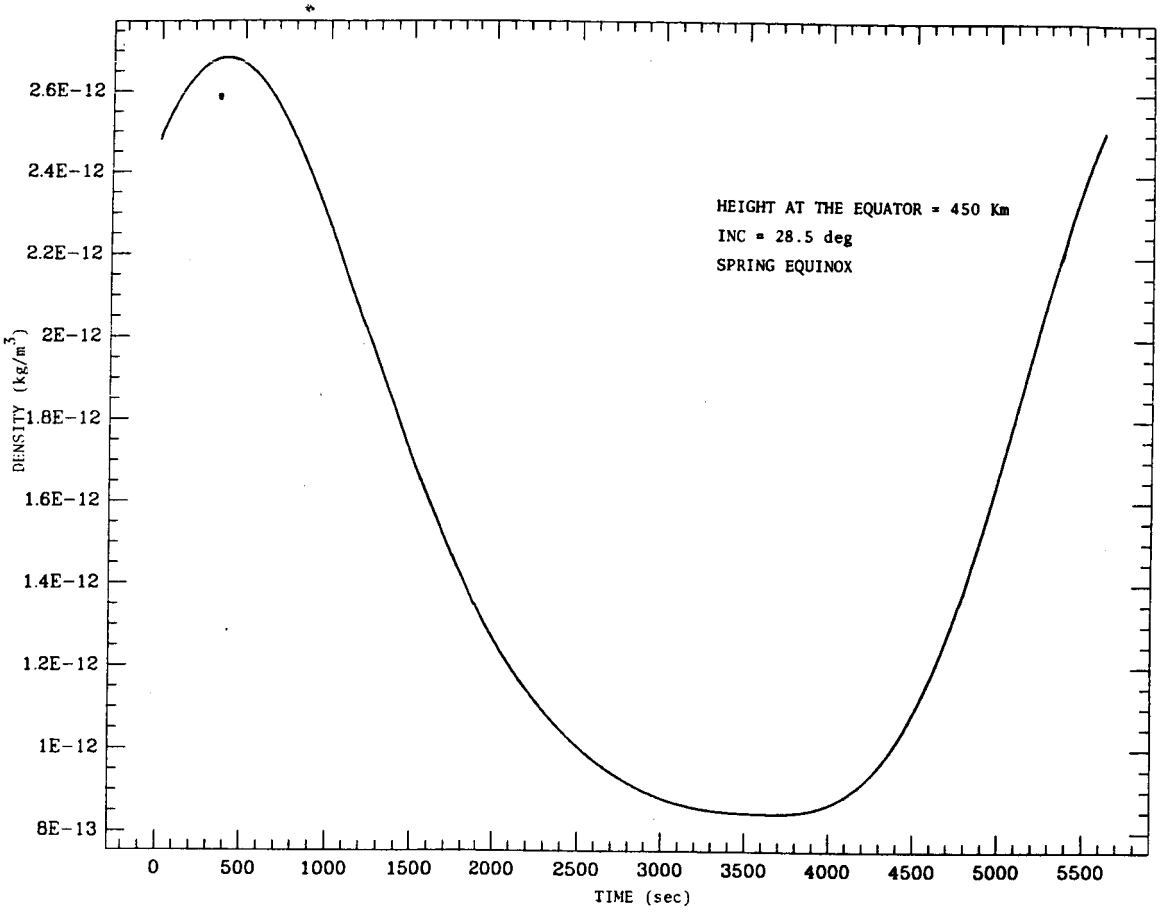

Figure 9a↑

Figure 9b↓

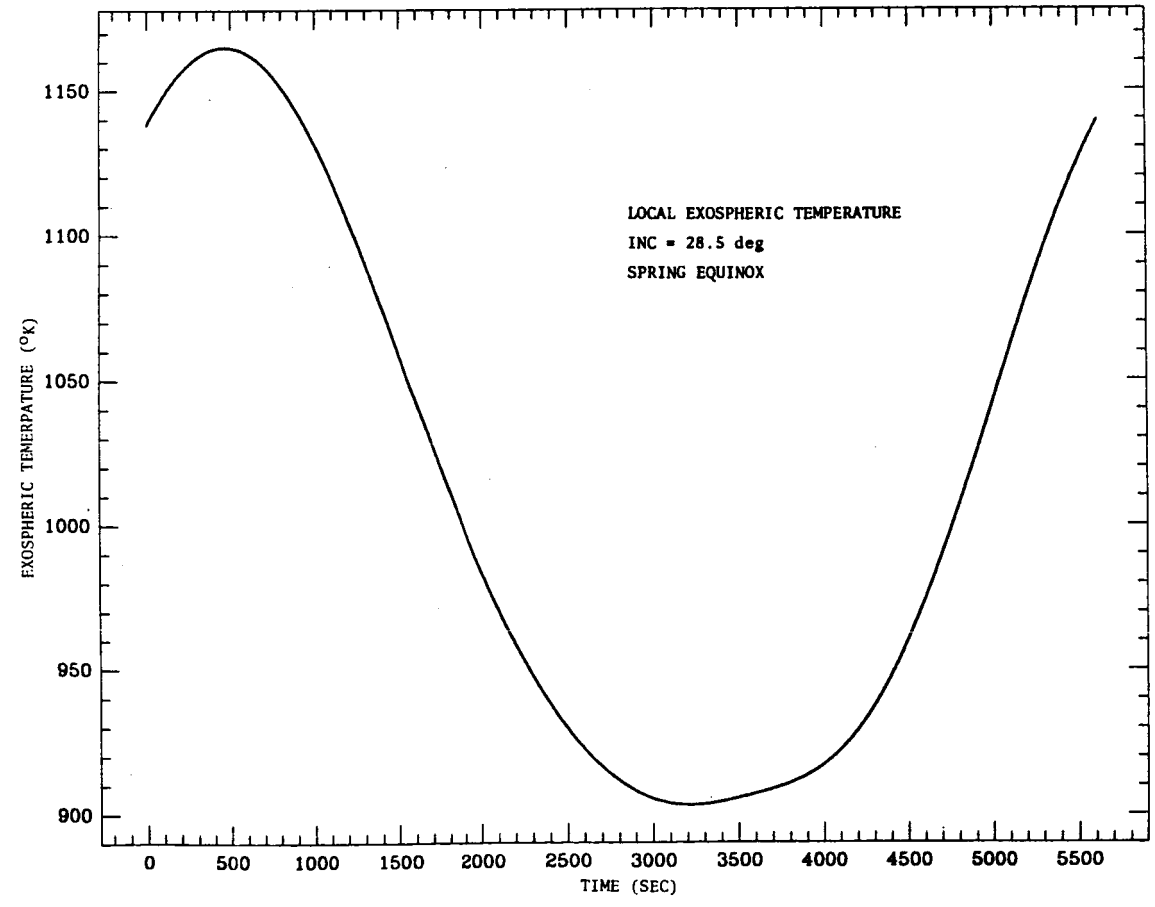

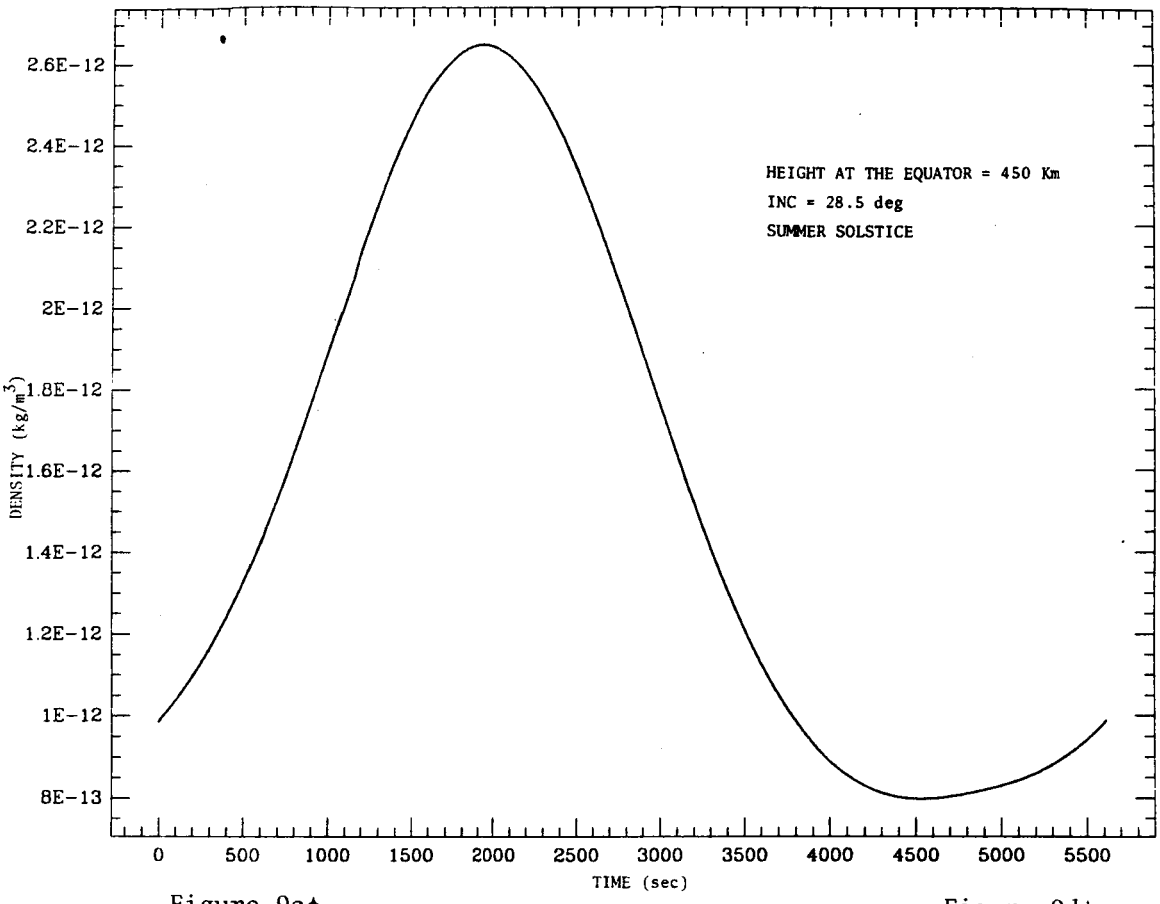

Figure 9c↑

Figure 9d↓

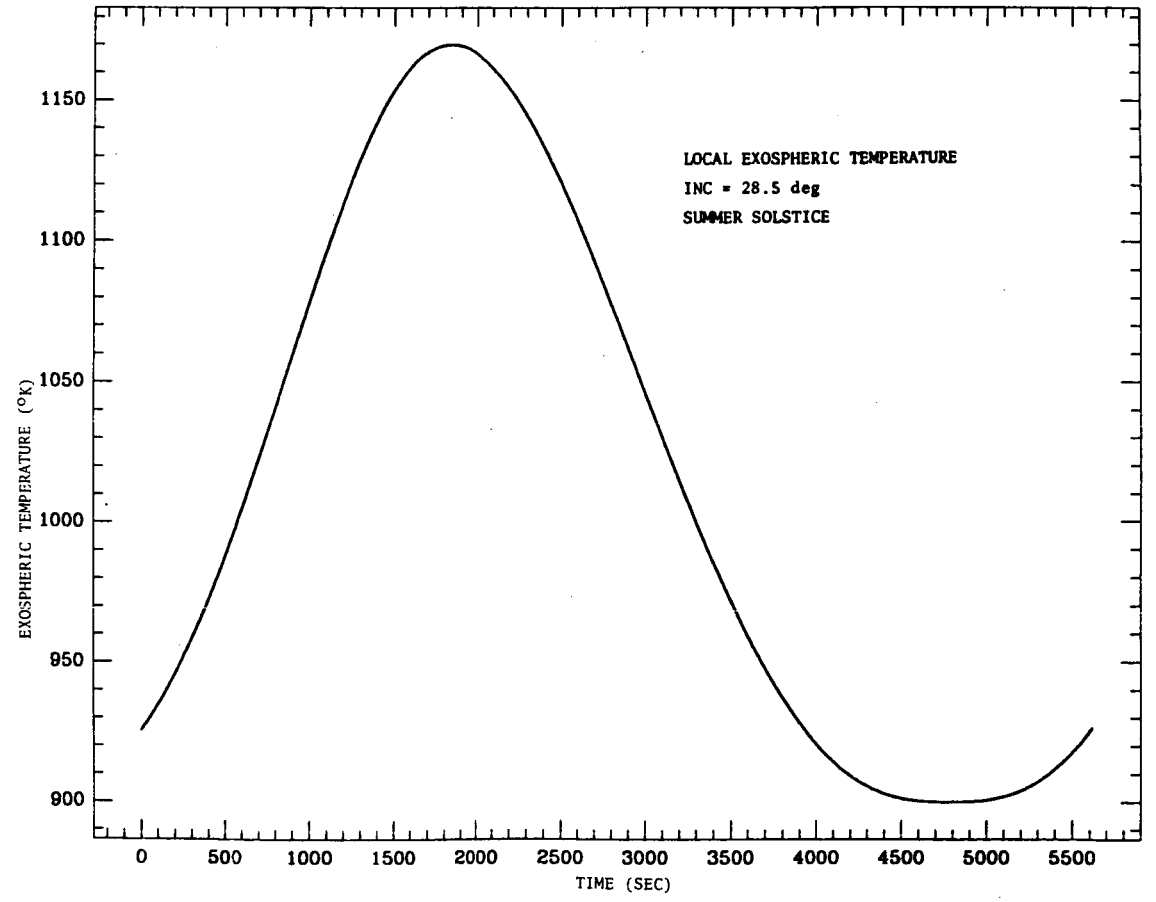

2.3.2 J_2 Model -

For satellites other than the geosynchronous ones the zonal harmonics of the Earth's gravity field are the major source of orbital perturbations. The expression of the potential of the Earth's gravity field for the i^{th}-mass of the system, limited to the zonal harmonic terms, is given by:

$$V_i = -\frac{\mu}{R_i}\left[1 - \sum_{n=1}^{\infty}\left(\frac{R_\oplus}{R_i}\right)^n J_n P_{no}(\sin\delta_i)\right] \qquad (2.3.10)$$

where $R_\oplus$ is the earth equatorial radius, μ the earth gravitational constant, J_n are the zonal harmonic coefficients, P_{no} are Legendre polinomials of argument $\sin\delta_i$, δ_i is the latitude of the i^{th}-mass and R_i is the radius vector of the same mass. If we limit the expansion of equation (2.3.10) to the J_2 term ($J_1 = 0$ in the geocentric reference frame) we obtain the expression of the J_2 perturbation potential as follows:

$$V_i^{J_2} = \frac{\mu}{R_i}\left(\frac{R_\oplus}{R_i}\right)^2 \frac{J_2}{2}\left(1 - 3\sin^2\delta_i\right) \qquad (2.3.11)$$

The gravity perturbation force due to J_2 is therefore given by:

$$\vec{F}_i^{J_2} = -\text{grad}\,(V_i^{J_2}) \qquad (2.3.12)$$

Since in functional form $V_i^{J_2} = V_i^{J_2}\left[R_i, \sin\delta_i(R_i)\right]$ we have:

$$F_{x_{ij}}^{J_2} = \left[\frac{\partial V_i^{J_2}}{\partial R_i} + \frac{\partial V_i^{J_2}}{\partial(\sin\delta_i)}\frac{\partial(\sin\delta_i)}{\partial R_i}\right]\frac{\partial R_i}{\partial x_{ij}} \qquad \begin{matrix} j = 1,2,3 \\ i = 1,\ldots,n \end{matrix} \qquad (2.3.13)$$

where $x_{i1} = X_i$, $x_{i2} = Y_i$, $x_{i3} = Z_i$ are the components of the radius vector R_i of the i^{th}-mass in the inertial reference frame. By substituting equation (2.3.11)

into equation (2.3.12) we finally get:

$$F_{X_i}^{J_2} = -\frac{3}{2}\,\mu\,J_2\,R_\oplus^2\,(1-5\sin^2\delta_i)\,\frac{X_i}{R_i^5}$$

$$F_{Y_i}^{J_2} = -\frac{3}{2}\,\mu\,J_2\,R_\oplus^2\,(1-5\sin^2\delta_i)\,\frac{Y_i}{R_i^5} \qquad (2.3.14)$$

$$F_{Z_i}^{J_2} = -\frac{3}{2}\,\mu\,J_2\,R_\oplus^2\,(3-5\sin^2\delta_i)\,\frac{Z_i}{R_i^5}$$

Figure 10 shows the components in inertial reference frame of the J_2 gravity force over one orbit with an inclination of 28°5 and an orbital altitude of 450 km. The components of the J_2 gravity force in inertial reference frame, given by equations (2.3.14), must be transformed into orbiting reference frame components in order to be introduced into our dynamics simulation computer code. This transformation is performed according to:

$$\left\{F_i^{J_2}\right\}_o = [T]\,\left\{F_i^{J_2}\right\}_I \qquad (2.3.15)$$

where the subscript (o) stands for orbiting reference fame and the subscript (I) stands for inertial reference frame. The transformation matrix [T] is given by:

$$[T] = \begin{bmatrix} \vec{i}\cdot\vec{I} & \vec{i}\cdot\vec{J} & \vec{i}\cdot\vec{K} \\ \vec{j}\cdot\vec{I} & \vec{j}\cdot\vec{J} & \vec{j}\cdot\vec{K} \\ \vec{k}\cdot\vec{I} & \vec{k}\cdot\vec{J} & \vec{k}\cdot\vec{K} \end{bmatrix} \qquad (2.3.16)$$

where $\vec{I}$, $\vec{J}$ and $\vec{K}$ are the unit vectors of the geocentric inertial reference frame while $\vec{i}$, $\vec{j}$ and $\vec{k}$ are the unit vectors of the orbiting reference frame given by:

$$\vec{i} = \frac{\vec{V}_o}{|V_o|}$$

$$\vec{k} = -\frac{\vec{R}_o}{|R_o|} \qquad (2.3.17)$$

$$\vec{j} = \vec{k} \times \vec{i}$$

where $\vec{R}_o$ is the radius vector of the origin of the orbiting reference frame and $\vec{V}_o$ is the velocity vector. The orbiting reference frame orbits the Earth at constant angular rate $\Omega = V_o/R_o$. Figure 11 shows the components of the J_2 gravity force in orbiting reference frame for the same case shown in the previous figure.

2.3.3 Thermal Model -

The thermal environment produces a periodical variation of the tether length (contractions and expansions) with consequent variations of the acceleration levels. The thermal inputs into the tether are:

A) Solar radiation

B) Earth albedo

C) Earth infrared radiation

D) Aerodynamic heating

E) Internal heating (i.e., Joule effect...)

The only cooling process is the radiation emitted by the wire. We have developed a new routine, neglecting the thermal inputs D and E, which calculates the temperature gradient of the tether per unit length as follows:

$$\dot{T} = \frac{Q^A + Q^B + Q^C - 2\pi r \sigma \epsilon T^4}{\bar{\rho}\ c\ m} \qquad (2.3.18)$$

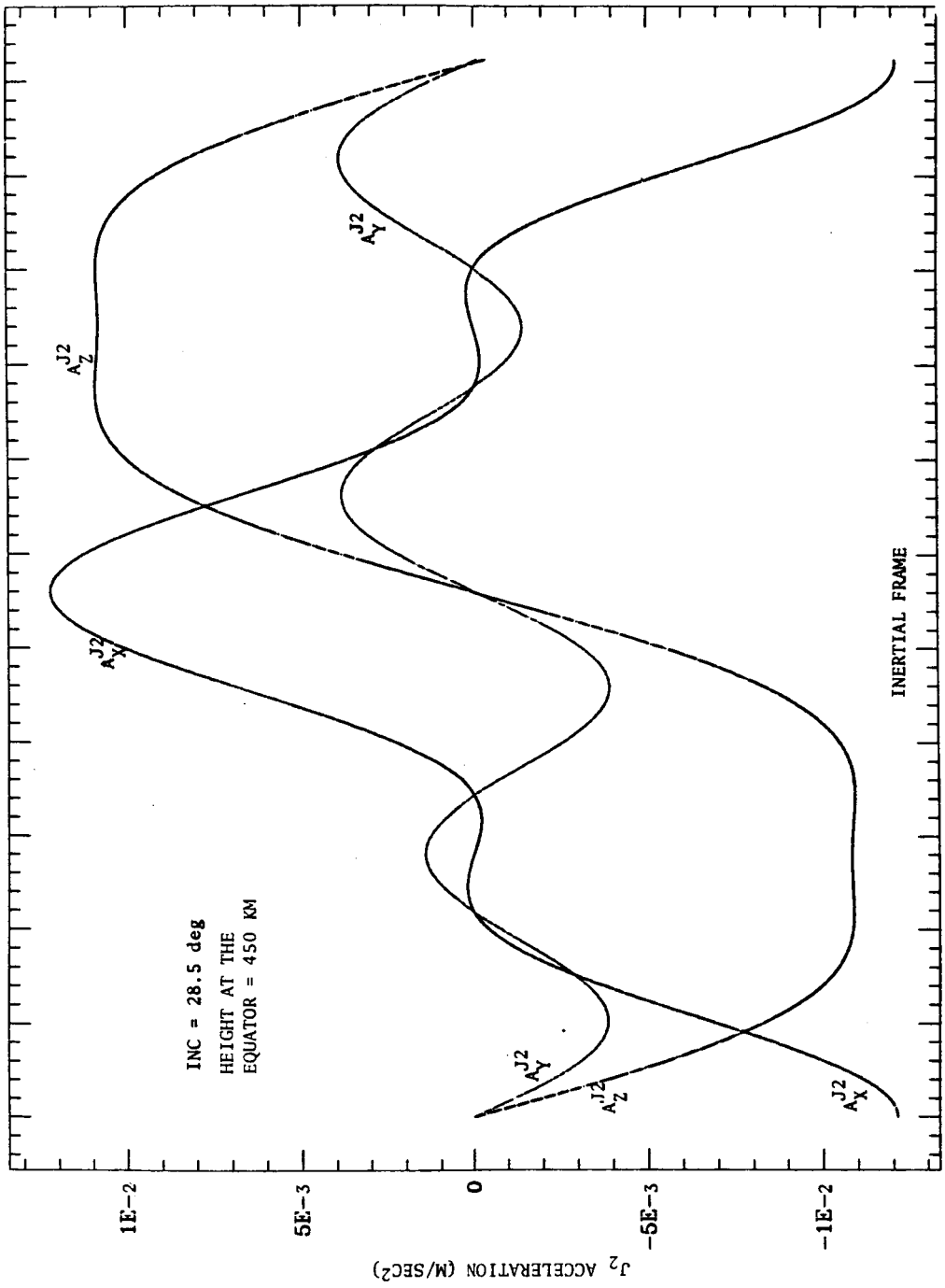
INC = 28.5 deg
HEIGHT AT THE
EQUATOR = 450 KM
INERTIAL FRAME
A_X^{J2}
A_Y^{J2}
A_Z^{J2}
A_Z^{J2}
A_Y^{J2}
A_X^{J2}
1E-2
5E-3
0
-5E-3
-1E-2
J_2 ACCELERATION (M/SEC^2)
0
500
1000
1500
2000
2500
3000
3500
4000
4500
5000
5500
TIME (SEC)

Figure 10.

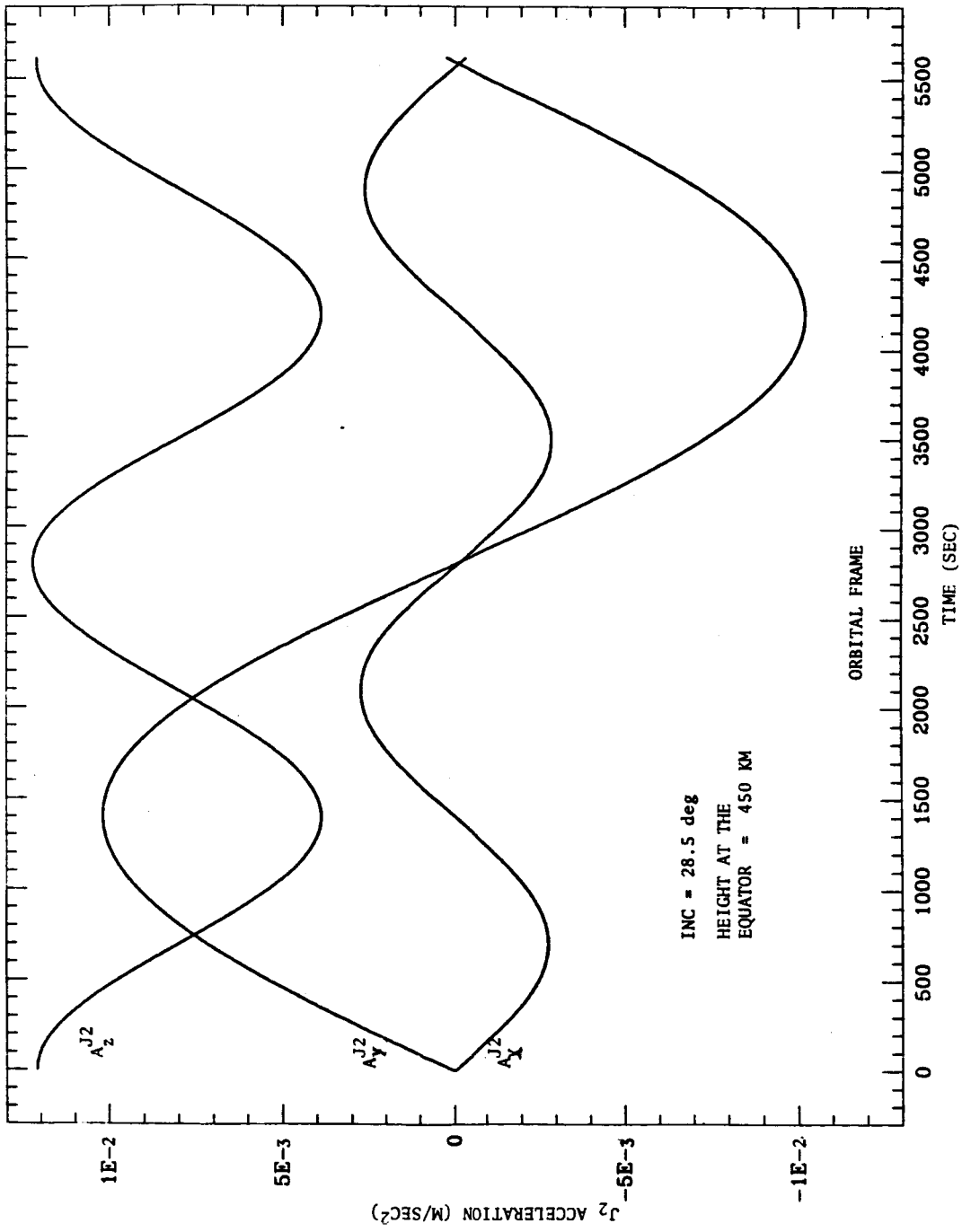
1E-2
5E-3
0
-5E-3
-1E-2
J_2 ACCELERATION (M/SEC^2)
A_Z^{J2}
A_Y^{J2}
A_X^{J2}
INC = 28.5 deg
HEIGHT AT THE
EQUATOR = 450 KM
ORBITAL FRAME
0
500
1000
1500
2000
2500
3000
3500
4000
4500
5000
5500
TIME (SEC)

Figure 11.

where:

r	=	tether radius
σ	=	Boltzman constant
ϵ	=	tether emissivity
$\overline{\rho}$	=	volume density of the tether
c	=	heat capacity of the tether
m	=	tether mass

For the expression of thermal inputs we have followed the line adopted by SKY-HOOK [4]. We included the earth albedo and we derived a more sophisticated model for the partial and the total eclipse of the wire [5]. The expressions of the Q^i are as follows:

$$\begin{aligned} Q^A &= 2\, r\, \alpha\, I^{SUN,INC} \\ Q^B &= a \cdot I^{SUN} \cdot \alpha \cdot r\ f \cdot \cos(\gamma) \\ Q^C &= 2\, \pi\, r\, \sigma\, \alpha_{IR}\ f\, T_{\oplus}^4 \end{aligned} \qquad (2.3.19)$$

where:

α	=	tether absorbitivity
a	=	earth albedo (annual average)
A	=	tether area
f	=	view factor $= \frac{\beta - \sin(2\,\beta)/2}{\pi}$ and $\sin\beta = \frac{R_{\oplus}}{R}$
γ	=	sun zenith angle
α_{IR}	=	infrared tether absorbitivity
$T_{\oplus}$	=	earth temperature

In the computation of Q^B and Q^C we neglected the solar declination angle, the differences between continental and ocean areas and the dependence with the

latitude and seasonal variations. We also assumed that the reflectance of the earth is isotropic and diffuse and that the spectral distribution of reflected radiation is equivalent to the spectral distribution of the incident radiation. We compared the thermal behavior of two different materials, under the same environmental conditions: stainless steel and kevlar. Figure 12 is a sketch of the geometry relevant to the thermal effects over the orbit. In Figure 13 and 14 the tether temperature is plotted vs. time (2 orbits) for a 2 mm diameter stainless steel and kevlar tether respectively. The initial temperature is the same for the two cases.

The thermal expansion (or contraction) of a tether segment of length ℓ_o is given by:

$$\Delta\ell = \alpha_T \ell_o \Delta T^{max} \qquad (2.3.20)$$

where α_T is the tether thermal expansion coefficient. If we assume a tether length of 10 km the expansion/contraction of the stainless steel wire and the kevlar wire over one orbit at 450 km altitude are respectively as follows:

$$|\Delta\ell_{steel}| \simeq 7m$$

$$|\Delta\ell_{kevlar}| \simeq 2m \qquad (2.3.21)$$

where we have assumed $\alpha_{T,steel} = 1.2\text{x}10^{-5}\ ^{\circ}K^{-1}$ and $\alpha_{T,kevlar} = -2\text{x}10^{-6}\ ^{\circ}K^{-1}$ while the maximum ΔT have been derived from the previous runs as follows: $|\Delta T_{steel}^{max}| \simeq 58^{\circ}K$ and $|\Delta T_{kevlar}^{max}| \simeq 95^{\circ}K$.

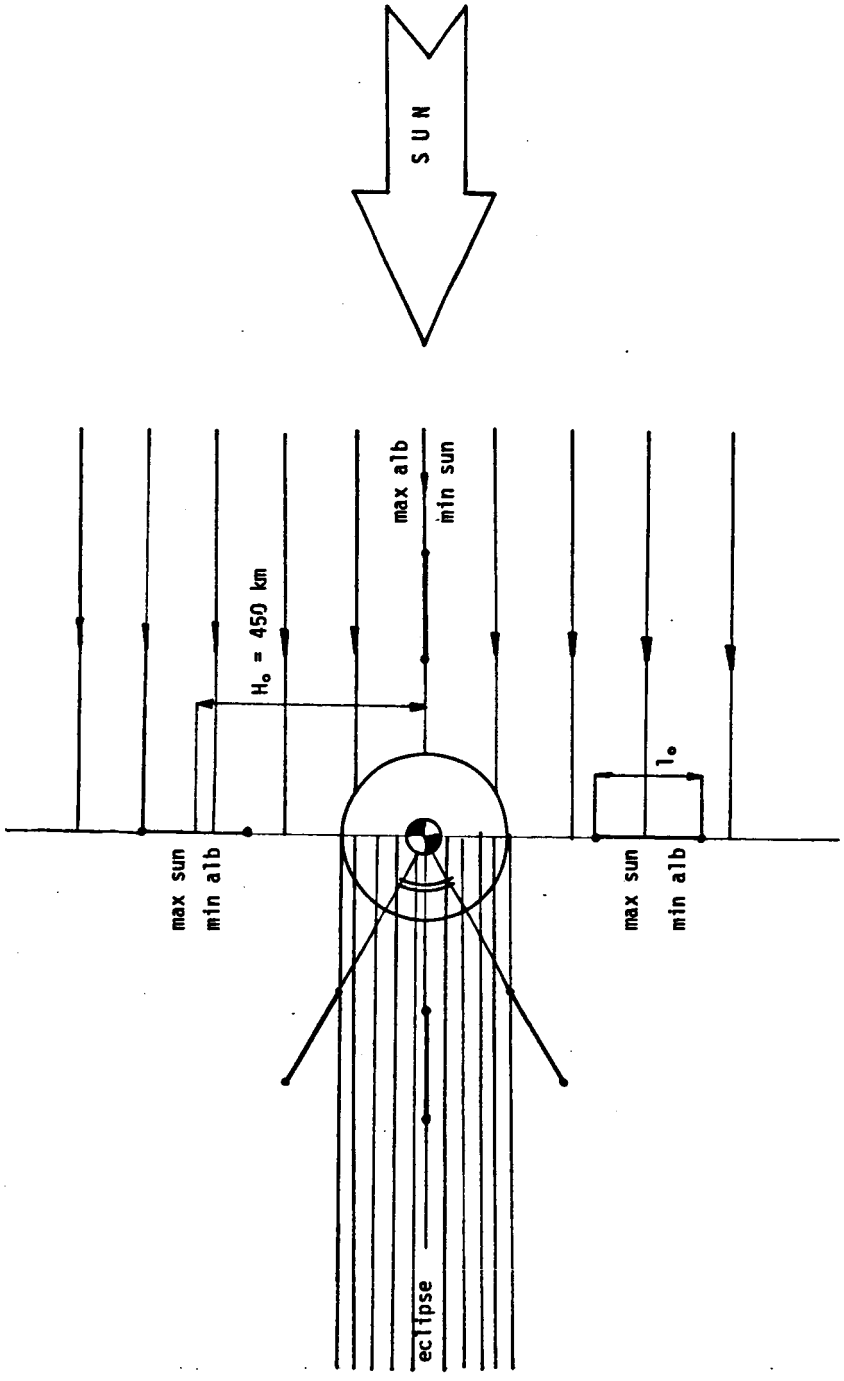
SUN
max alb
min sun
H_o = 450 km
l_o
max sun
min alb
max sun
min alb
eclipse

Figure 12.

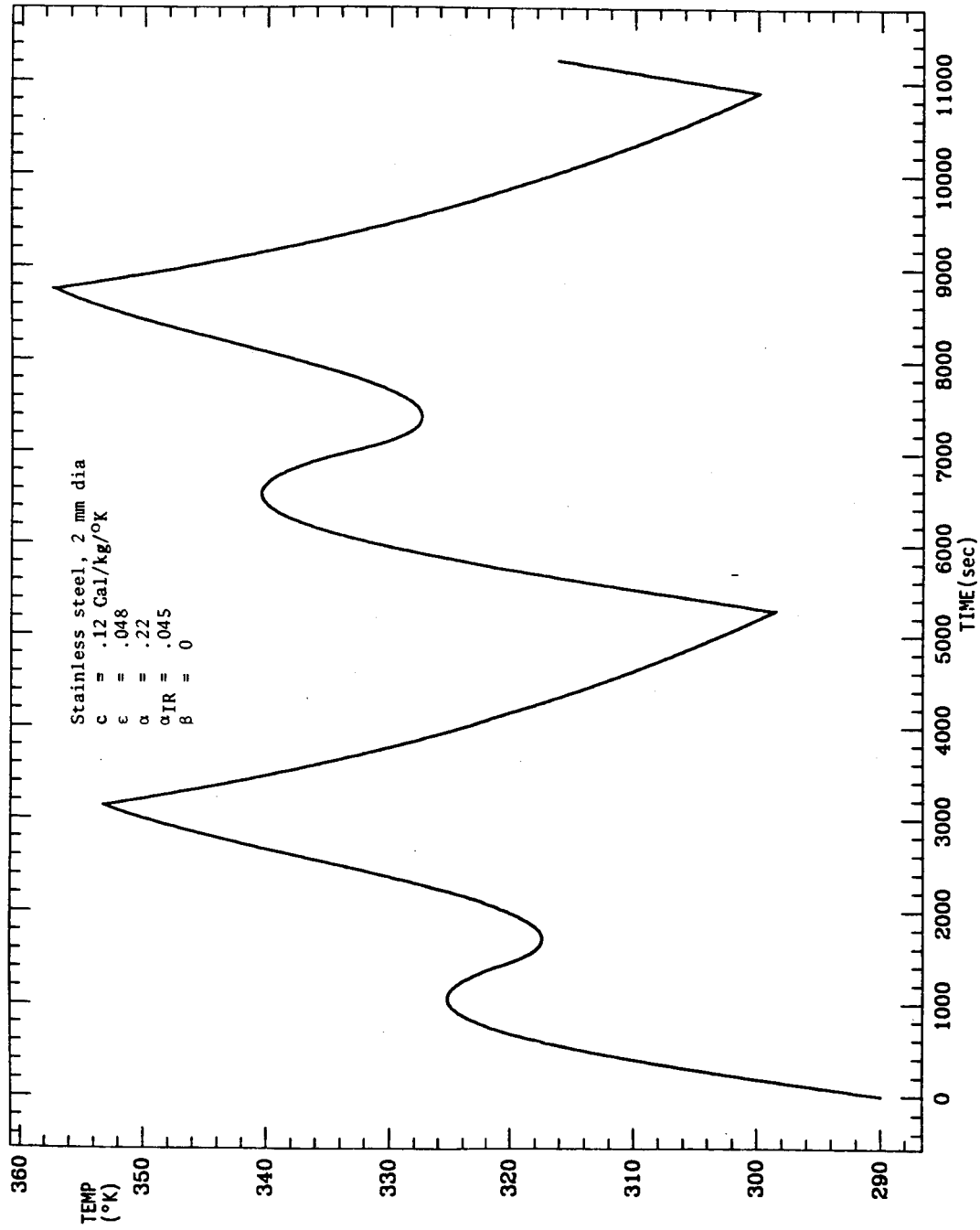
Stainless steel, 2 mm dia
c = .12 Cal/kg/°K
ε = .048
α = .22
αIR = .045
β = 0
TEMP (°K)
360
350
340
330
320
310
300
290
0
1000
2000
3000
4000
5000
6000
7000
8000
9000
10000
11000
TIME(sec)

Figure 13.

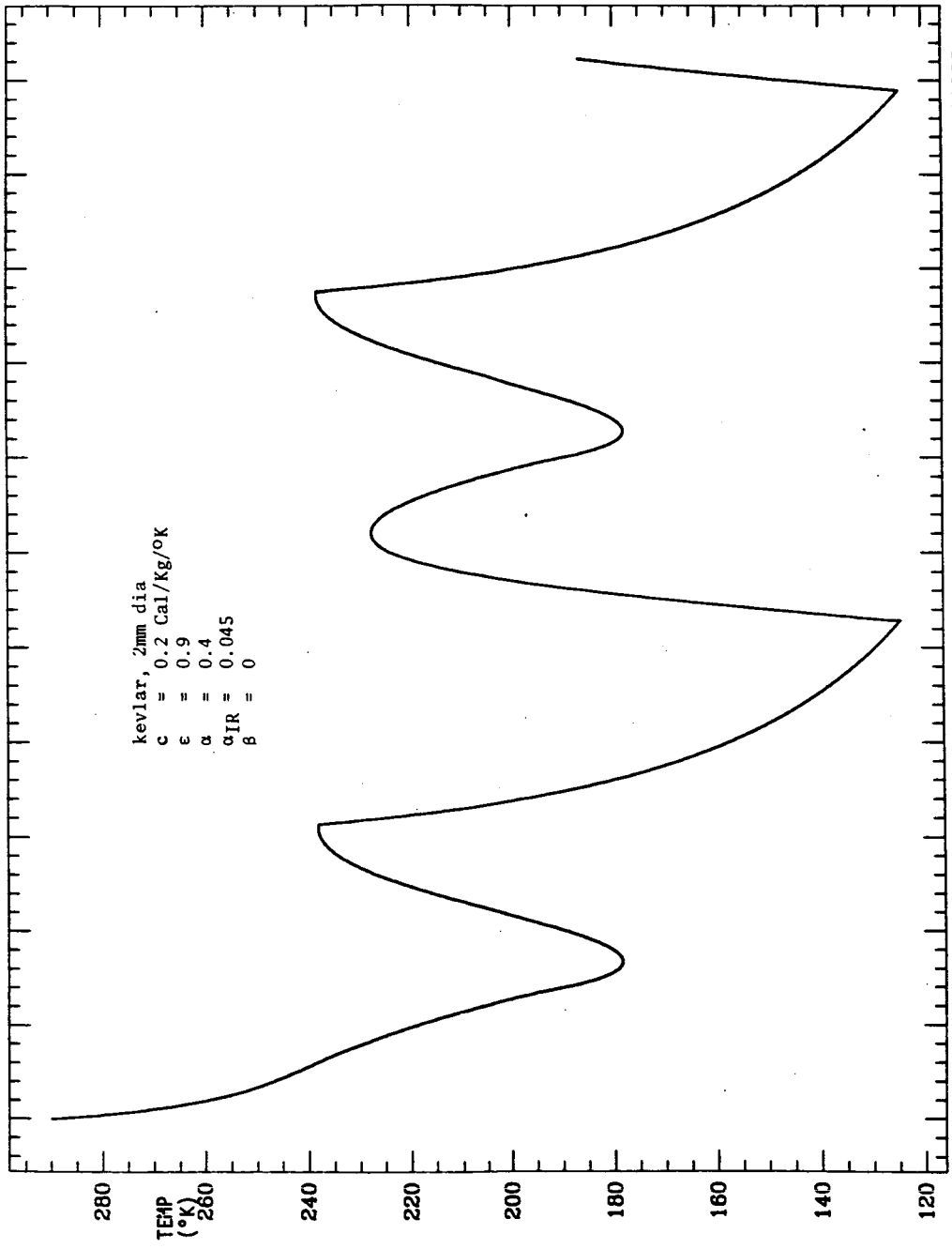
kevlar, 2mm dia
c = 0.2 Cal/Kg/°K
ε = 0.9
α = 0.4
α_{IR} = 0.045
β = 0
TEMP (°K)
280
260
240
220
200
180
160
140
120
0
1000
2000
3000
4000
5000
6000
7000
8000
9000
10000
11000
TIME(sec)

Figure 14.

References for Section 2.3

[1] C.E. Roberts. "An Analytical Model for Upper Atmosphere Densities Based Upon Jacchia's 1970 Models." Celestial Mechanics, Vol. 4, pp. 378"-377, 1971.

[2] L.G. Jacchia. "Thermospheric Temperature, Density and Composition: New Models." SAO Report SR375, March 1977.

[3] COSPAR Working Group 4, "CIRA. COSPAR International Reference Atmosphere 1972." Akademie-Verlag, Berlin, 1972

[4] Kalaghan, P.H., D.A. Arnold, G. Colombo, M.D. Grossi, L.R. Kirschner and O. Orringer. "Study of the Dynamics of a Tethered Satellite System (SKYHOOK)." Final Report NAS8-32199, SAO, March 1978.

[5] __. "Spacecraft Attitude, Determination and Control." Edited by James R. Wertz, Reidel Publishing Company.

2.4 Concluding Remarks

A survey of various out-of-plane libration control laws has been carried out. Consequently a yo-yo control law with amplitude of the tether length variation proportional to the amplitude of the out-of-plane libration has been selected. This control law provides good damping when applied to a (theoretical) two-dimensional system. In the actual 3-dimensional 4-mass tethered system, however, energy is transferred to the least damped degrees of freedom (the out-of-plane lateral deflections are still undamped in the present simulations) in such a way as to decrease the effectiveness of the algorithm for out-of-plane libration control. The addition of damping algorithms for the out-of-plane lateral deflections is therefore necessary (these damping algorithms will be developed in the next reporting period).

A completely new package of major environmental disturbances relevant to the altitude range of the Space Station has been also developed. This package consists of: a new drag model based on Jacchia's 1977 model, a thermal model of

the wire and a model of the J_2 gravity perturbation.

3.0 PROBLEMS ENCOUNTERED DURING REPORTING PERIOD

None

4.0 ACTIVITY PLANNED FOR THE NEXT REPORTING PERIOD

In the next reporting period the algorithms for damping the out-of-plane lateral oscillations will be developed. The investigation of the forced dynamics of the 4-mass tethered system during the station-keeping phase will also be carried out.